Cell Reports

Article

# Dysregulation of *Streptococcus pneumoniae* zinc homeostasis breaks ampicillin resistance in a pneumonia infection model

## Graphical abstract

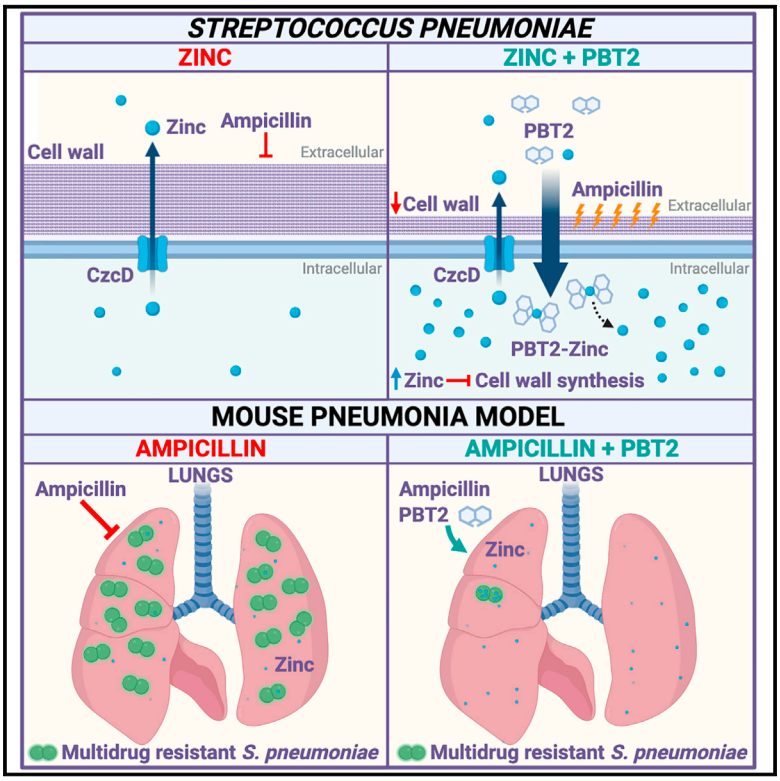


## Highlights

- Zinc can impair the activity of the peptidoglycan biosynthetic enzyme GlmU
- The zinc ionophore PBT2 overwhelms *S. pneumoniae* zinc resistance mechanisms
- PBT2-mediated zinc intoxication breaks resistance to multiple antibiotic classes
- PBT2 rescues ampicillin efficacy during drug-resistant *S. pneumoniae* lung infection

## Authors

Erin B. Brazel, Aimee Tan, Stephanie L. Neville, ..., Mark J. Walker, Jason W. Rosch, Christopher A. McDevitt

## Correspondence

christopher.mcdevitt@unimelb.edu.au

## In brief

Antibiotic resistance is a growing threat to treatment of pneumonia caused by *Streptococcus pneumoniae*. Brazel et al. show how zinc can be used to break bacterial antibiotic resistance. They repurpose the safe-for-human-use zinc transporting ionophore, 5,7-dichloro-2-[(dimethylamino)methyl]quinolin-8-ol (PBT2), to break bacterial drug resistance during lung infection and restore the efficacy of ampicillin treatment.

Brazel et al., 2022, Cell Reports *38*, 110202
January 11, 2022 
https://doi.org/10.1016/j.celrep.2021.110202

CellPress

Cell Reports

CellPress
OPEN ACCESS

Article

# Dysregulation of *Streptococcus pneumoniae* zinc homeostasis breaks ampicillin resistance in a pneumonia infection model

Erin B. Brazel,[1] Aimee Tan,[2] Stephanie L. Neville,[2] Amy R. Iverson,[3] Saumya R. Udagedara,[4] Bliss A. Cunningham,[2] Mwilye Sikanyika,[5] David M.P. De Oliveira,[6] Bernhard Keller,[6] Lisa Bohlmann,[6] Ibrahim M. El-Deeb,[7] Katherine Ganio,[2] Bart A. Eijkelkamp,[1,8] Alastair G. McEwan,[6] Mark von Itzstein,[7] Megan J. Maher,[4,5,9] Mark J. Walker,[6,9] Jason W. Rosch,[3,9] and Christopher A. McDevitt[1,2,9,10,*]

[1]Department of Molecular and Biomedical Science, School of Biological Sciences, University of Adelaide, Adelaide, SA 5005, Australia
[2]Department of Microbiology and Immunology, The Peter Doherty Institute for Infection and Immunity, The University of Melbourne, Melbourne, VIC 3000, Australia
[3]Department of Infectious Diseases, St Jude Children's Research Hospital, Memphis, TN 38105, USA
[4]School of Chemistry and the Bio21 Molecular Science and Biotechnology Institute, The University of Melbourne, Melbourne, VIC 3000, Australia
[5]Department of Biochemistry and Genetics, La Trobe Institute for Molecular Science, La Trobe University, Melbourne, VIC 3083, Australia
[6]School of Chemistry and Molecular Biosciences and Australian Infectious Diseases Research Centre, The University of Queensland, QLD 4072, Australia
[7]Institute for Glycomics, Griffith University, QLD 4222, Australia
[8]Present address: College of Science and Engineering, Flinders University, SA 5042, Australia
[9]These authors contributed equally
[10]Lead contact
*Correspondence: christopher.mcdevitt@unimelb.edu.au
https://doi.org/10.1016/j.celrep.2021.110202

## SUMMARY

*Streptococcus pneumoniae* is the primary cause of community-acquired bacterial pneumonia with rates of penicillin and multidrug-resistance exceeding 80% and 40%, respectively. The innate immune response generates a variety of antimicrobial agents to control infection, including zinc stress. Here, we characterize the impact of zinc intoxication on *S. pneumoniae*, observing disruptions in central carbon metabolism, lipid biogenesis, and peptidoglycan biosynthesis. Characterization of the pivotal peptidoglycan biosynthetic enzyme GlmU indicates a sensitivity to zinc inhibition. Disruption of the sole zinc efflux pathway, *czcD*, renders *S. pneumoniae* highly susceptible to β-lactam antibiotics. To dysregulate zinc homeostasis in the wild-type strain, we investigated the safe-for-human-use ionophore 5,7-dichloro-2-[(dimethylamino) methyl]quinolin-8-ol (PBT2). PBT2 rendered wild-type *S. pneumoniae* strains sensitive to a range of antibiotics. Using an invasive ampicillin-resistant strain, we demonstrate in a murine pneumonia infection model the efficacy of PBT2 + ampicillin treatment. These findings present a therapeutic modality to break antibiotic resistance in multidrug-resistant *S. pneumoniae*.

## INTRODUCTION

*Streptococcus pneumoniae*, also termed the pneumococcus, is a World Health Organization high priority bacterial pathogen and the primary cause (≤50% of cases) of community-acquired bacterial pneumonia (CABP), with *Haemophilus influenzae* and *Moraxella catarrhalis* the other major etiological agents (Cilloniz et al., 2018; World Health Organization, 2003, 2010). CABP is a leading cause of morbidity, mortality, and economic burden worldwide. Although commonly associated with the young and elderly, it also represents a significant, although under-appreciated, burden in working-age adults (18–64 years old). Annually, CABP infections in working-age adults, especially those with co-morbidities, account for more than 5.6 million infections in the United States, with an estimated economic cost of more than US$10 billion annually in direct and indirect costs (Amin et al., 2014; Bonafede et al., 2012; Polsky et al., 2012). The burden of CABP in Indigenous populations can be much higher. In Australia, Aboriginal and Torres Strait Islander populations have a 4-fold greater hospitalization rate and up to an 11-fold greater mortality rate than in non-Indigenous populations (Basnayake et al., 2017; O'Grady et al., 2018). Non-severe CABP is treated without hospitalization or identification of the infectious agent by frontline antibiotics, primarily monotherapy with a β-lactam, macrolide, or fluoroquinolone. However, the efficacy of this approach is waning, with a recent study of CABP reporting a treatment failure of approximately 25% for patients receiving β-lactam antibiotic monotherapy (McKinnell et al., 2017).

Treatment failure can be attributed to antibiotic resistance, although other factors, such as co-morbidities, may also contribute (Peyrani et al., 2019). An inability to treat infections that occur in healthy community populations is a major threat to human health and presents an opportunity for the further dissemination of antibiotic resistance determinants. Accordingly, overcoming or preventing loss of frontline antibiotic treatment efficacy is crucial in order to reduce the health and economic burden of CABP.

Resistance to pneumococcal infection and pneumonia is significantly influenced by the zinc (Zn) status of the host (Strand et al., 2001, 2003). During the acute phase response, Zn is mobilized from the blood into the lungs and other tissues and contributes to the efficacy of host control of infection (Haase and Rink, 2014). Notably, a recent study of *S. pneumoniae* infection in mice using elemental bio-imaging revealed spatially complex Zn flux and the emergence of Zn-enriched regions (Eijkelkamp et al., 2019). Concomitant with Zn influx, the pathogen demonstrated a pattern of gene regulation indicative of Zn stress. Limitation of dietary Zn intake, and impaired Zn mobilization during infection, resulted in increased susceptibility to *S. pneumoniae*-mediated pneumonia and invasive disease. Accordingly, we sought to understand how Zn stress impacts *S. pneumoniae* and how the innate antimicrobial activity of Zn might be harnessed to enhance the control of infection. Here, we report the molecular basis by which Zn contributes to the breakage of resistance to β-lactam antibiotics in *S. pneumoniae*. We then repurpose the orally bioavailable hydroxyquinoline-based ionophore PBT2 (5,7-dichloro-2-[(dimethylamino)methyl]quinolin-8-ol), which is able to mediate the transfer of divalent Zn ions across biological membranes (Bohlmann et al., 2018) to break *S. pneumoniae* antibiotic resistance *in vitro* and in an *in vivo* murine model of lung infection, demonstrating the therapeutic rescue of a frontline antibiotic class.

## RESULTS

An investigation of the transcriptional impact of Zn stress in *S. pneumoniae* strain D39 revealed that 54 genes had altered patterns of expression, including those involved in genetic competence, the Leloir pathway for the catabolism of galactose, manganese (Mn) import, and Zn homeostasis (>2-fold; Figure 1A, Table S1). A metabolomic analysis of the pneumococcus under Zn stress revealed disruptions in numerous pathways, including central carbon metabolism, glutathione abundance, polyamine biosynthesis (Figure 1B), cell membrane, and cell wall and capsule biogenesis pathways (Table S2). Notably, Zn stress seemed to impact peptidoglycan biosynthesis as indicated by a 4.9-fold increase in accumulation of glucosamine 6-phosphate and significant reductions in *N*-acetyl-D-glucosamine-1-phosphate (2.9-fold), acetyl-coenzyme A (CoA) (3.7-fold), and UDP-*N*-acetyl-D-glucosamine (1.5-fold) (Figure S1A, Table S2). Glucosamine 6-phosphate is a precursor in peptidoglycan production that is converted to UDP-*N*-acetyl-D-glucosamine via the concerted actions of GlmM and GlmU, enzymes essential for the viability of *S. pneumoniae* (van Opijnen and Camilli, 2012) (Figure 1C). These enzymes have been prominent targets for antimicrobial development owing to their pivotal roles in peptidoglycan and lipopolysaccharide biosynthesis pathways in Gram-positive and Gram-negative pathogens (Kostrewa et al., 2001; Li et al., 2011; Rani and Khan, 2016). Zn stress did not affect expression of the genes encoding GlmM, GlmU, or GlmS, suggesting that the metal might be perturbing protein function. As the intermediate product glucosamine 1-phosphate was not assessed by the metabolomic analyses, we directly investigated the impact of Zn on GlmM and GlmU function. Zn had no effect on the isomerase activity of GlmM (Figure S1B). GlmU is an essential bifunctional metalloenzyme, with both acetyltransferase and uridyltransferase activities. Zn binding significantly impaired the acetyltransferase-specific activity of GlmU (Figure 1D), while the uridyltransferase specific activity was disrupted to a lesser extent (Figure 1E), consistent with metabolite analyses. To further elucidate the impact of Zn on GlmU, the high-resolution crystal structure of the protein was determined in the presence of Zn (Figures 1F, S1C, and S1D, Table 1). The structure revealed that Zn bound in the acetyltransferase domain of GlmU via coordination to residues Glu315 and His330, and two water ligands. This pair of charged residues is highly conserved in more than 98% (Glu315) and 99% (His330) of 20,010 *S. pneumoniae* genomes (Figure 1G) (Gladstone et al., 2019). Notably, this site is distinct from the essential magnesium binding site, which is located in the uridyltransferase domain and composed of the residues Asp102 and Asn227, and oxygen atoms from the substrate (Kostrewa et al., 2001). The role of Glu315 and His330 in Zn ligation was investigated by mutation to Ala. The $GlmU_{E315A/H330A}$ variant retained activity (Figures 1H and 1I), but showed negligible Zn binding (Figure S1E) and was insensitive to Zn-mediated perturbation of acetyltransferase-specific activity (Figure 1H).

Given the pivotal role of GlmU in the peptidoglycan biosynthetic pathway and the *in vitro* impact of Zn intoxication on enzymatic function, the efficacy of cell-wall targeting antibiotics was examined. However, treatment with concentrations of up to 100 μM Zn did not enhance antibiotic activity against *S. pneumoniae* (Figure S1F). We hypothesized that this was attributable to the function of the cation diffusion facilitator protein CzcD (Kloosterman et al., 2007), which is the sole efflux transporter upregulated upon exposure to Zn stress (Figure 1A). Accordingly, an isogenic deletion mutant was generated and the impact on resistance to Zn stress determined. The D39 Δ*czcD* strain was more susceptible to Zn stress, but not to nickel or copper stress, than the wild-type strain (Figures 2A and 2B, S2). Further, whole cell metal content analyses revealed that the D39 Δ*czcD* strain accumulated more Zn upon exposure to exogenous Zn, which occurred concomitantly with dysregulation of Mn homeostasis (Figures 2C and 2D). The latter impact can be ascribed to the established susceptibility of pneumococcal Mn import to competitive inhibition by exogenous Zn (McDevitt et al., 2011). Transcriptomic analysis of the D39 Δ*czcD* strain (Figure 2E, Table S1) revealed that Zn stress exerted a greater impact on the mutant, with 228 genes showing altered patterns of expression, 26 (of 54; 48%) of which were shared with the D39 wild-type strain (Table S3). We then examined the sensitivity of the Δ*czcD* mutant to antibiotic treatment and observed reduced survival of the mutant strain in comparison with wild type upon exposure to the combination of Zn and penicillin ($p < 0.01$, two-tailed unpaired *t* test) (Figure S1F).

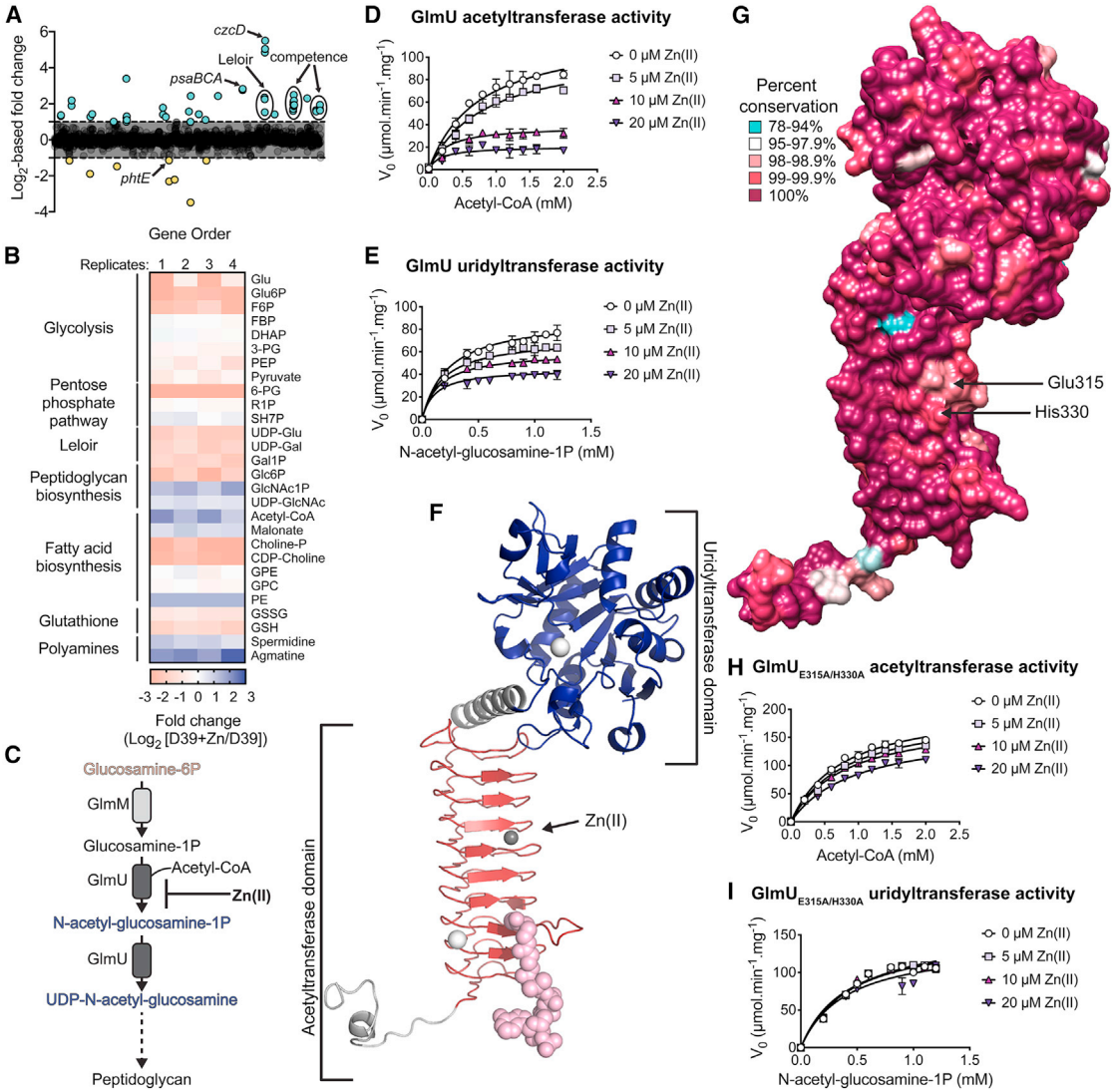


**Figure 1. Zinc intoxication broadly perturbs *S. pneumoniae* metabolism and the peptidoglycan biosynthesis enzyme GlmU**

(A) RNA sequencing of *S. pneumoniae* D39 to determine relative gene expression of Zn-treated cultures compared to untreated, expressed as $\log_2$-fold change. Each dot represents a gene, distributed on the x axis in accordance with locus tag numbering for D39. Genes more highly expressed in the presence of 100 μM $ZnSO_4$ are present above the x axis (blue), with those below the x axis expressed at a lower level (yellow). Genes of interest are annotated with their putative or characterized functions.

(B) Heatmap of changes in relative abundance of *S. pneumoniae* D39 key metabolites upon exposure to 100 μM $ZnSO_4$. Each row represents a metabolite and each column represents an independent biological sample (n = 4). The relative abundance value of each sample metabolite is plotted in blue-pink color scale, where the pink color of the tile represents increased abundance and blue indicates decreased abundance.

(C) Biosynthetic pathway involving GlmM and GlmU with the relative abundance of key metabolites shown (color scheme as in B) and the impact of Zn.

(D and E) Spectrophotometric analysis of GlmU acetyltransferase activity (D) or uridyltransferase activity (E) in the presence of increasing Zn concentrations. Data are fit by nonlinear regression using the Michaelis-Menten (D) or uncompetitive inhibition (E) kinetic models with individual data points representing the mean (± standard error of the mean) of triplicate analyses.

(F) GlmU structure (PDB ID: 7KR9) determined to 1.90 Å resolution shown in cartoon representation in complex with acetyl-CoA (light pink spheres), calcium (white spheres) and Zn (gray sphere). The uridyltransferase domain is represented in blue and the acetyltransferase domain in red, with the linking helix and C-terminal extension in gray.

(G) Global amino acid variation of *S. pneumoniae* GlmU mapped against the Zn-bound crystal structure (F). Frequency of residue conservation from 20,010 *S. pneumoniae* GlmU sequences represented as a color gradient. Thresholds were chosen to represent differing orders of magnitude for conservation, with thresholds set at 94%, 98%, 99%, and 100% sequence conservation at the residue. The locations of Glu315 and His330 are indicated by arrows.

(H and I) Spectrophotometric analysis of $GlmU_{E315A/H330A}$ acetyltransferase activity (H) or uridyltransferase activity (I) in the presence of increasing Zn concentrations. Data are fit by nonlinear regression using the Michaelis-Menten enzyme kinetic model with individual data points representing the mean (± standard error of the mean) of triplicate analyses.

**Table 1. Diffraction data collection and refinement statistics**[a]

| Data collection | | | |
|---|---|---|---|
| Dataset | Native | High energy | Low energy |
| Wavelength (Å) | 0.9537 | 1.240 | 1.305 |
| Temperature (K) | 100 | | |
| Diffraction source | Australian Synchrotron MX2 | | |
| Detector | EIGER X 16M | | |
| Space group | *R*32 | | |
| *a*, *b*, *c* (Å) | 92.9, 92.9, 281 | 92.9, 92.9, 281 | 93.0, 93.0, 281 |
| α, β, γ (°) | 90, 90, 120 | | |
| Resolution range (Å) | 47.0–1.90 | 47.0–2.47 | 47.0–2.60 |
| | (1.94–1.90) | (2.57–2.47) | (2.72–2.60) |
| Total no. of reflections | 382,291 (24,211) | 173,744 (19,946) | 148,618 (18,286) |
| No. of unique reflections | 37,206 (2319) | 17,175 (1918) | 14,797 (1771) |
| Completeness (%) | 99.9 (98.8) | 100 (99.9) | 99.9 (99.6) |
| Redundancy | 10.3 (10.4) | 10.1 (10.4) | 10.0 (10.3) |
| $\langle I/\sigma(I)\rangle$ | 18.2 (3.1) | 29.7 (11.7) | 33.4 (14.9) |
| $R_{merge}$ (%) | 5.40 (54.1) | 3.90 (11.9) | 3.5 (8.8) |
| $R_{pim}$ (%) | 1.80 (17.5) | 4.10 (12.6) | 1.2 (2.9) |
| **Refinement** | | | |
| Dataset | | Native | |
| Resolution range (Å) | | 47.0–1.90 (1.95–1.90) | |
| No. of reflections, working set | | 35,343 (2572) | |
| No. of reflections, test set | | 1862 (144) | |
| $R_{work}$ (%) | | 18.5 (21.9) | |
| $R_{free}$ (%) | | 22.7 (26.1) | |
| Rmsd bond lengths (Å) | | 0.007 | |
| Rmsd bond angles (°) | | 1.551 | |
| Ramachandran[b] | | | |
| Favored, % | | 98.7 | |
| Allowed, % | | 1.3 | |
| PDB ID code | | 7KR9 | |

[a]Values in parentheses are for the highest resolution shell.
[b]Calculated using MolProbity.

This observation suggested that disruption of Zn homeostasis in wild-type *S. pneumoniae* might promote sensitivity to antibiotics. Accordingly, we investigated the Zn-binding ionophore PBT2, which facilitates the direct permeation of Zn ions across biological membranes. PBT2 is an orally bioavailable hydroxyquinoline-based ionophore that has progressed to phase II human clinical trials for the treatment of Huntington's and Alzheimer's diseases, with once-daily doses of 250 mg generally safe and well-tolerated when administered for periods of 6–24 months (Bush, 2013; Huntington Study Group Reach, 2015; Lannfelt et al., 2008; Villemagne et al., 2017). Here, the ability of PBT2 to enhance Zn intoxication of wild-type *S. pneumoniae* was first investigated. Growth of D39 wild-type and Δ*czcD* strains were similar in the presence of 50 μM Zn or PBT2 (0.5 μM or 1 μM; Figures 2A and 2B). The combination of 50 μM Zn and 0.5 μM PBT2 perturbed growth of the wild-type strain, while growth was abrogated upon supplementation with 50 μM Zn and 1 μM PBT2. The Δ*czcD* strain was severely impaired by both PBT2 + Zn supplementation combinations (Figures 2A and 2B). Consistent with thesephenotypic observations, pneumococcal Mn and Zn homeostasis was dysregulated in PBT2 + Zn-treated wild-type *S. pneumoniae* D39 (Figures 2C and 2D) with other elements unaffected (Figures S3A–S3D). Whole cell metal accumulation revealed that Mn homeostasis was severely disrupted (Figure 2C), although this seemed to be mediated by Zn treatment and independent of PBT2 in the experimental conditions used. Consistent with this inference, an *S. pneumoniae* D39 strain encoding a fluorescent reporter regulated by the Mn-dependent regulator PsaR (which facilitates *psaBCA* transcription in response to Mn deprivation) showed increased fluorescence in response to Zn and PBT2 + Zn treatment, but not PBT2 alone (Figure 2F). Zn accumulation was significantly elevated in wild-type *S. pneumoniae* D39 treated with PBT2 + Zn compared with PBT2- or Zn-treated controls and reached levels comparable with the Zn-intoxicated Δ*czcD* strain (Figure 2D). An analysis of an *S. pneumoniae* D39 strain

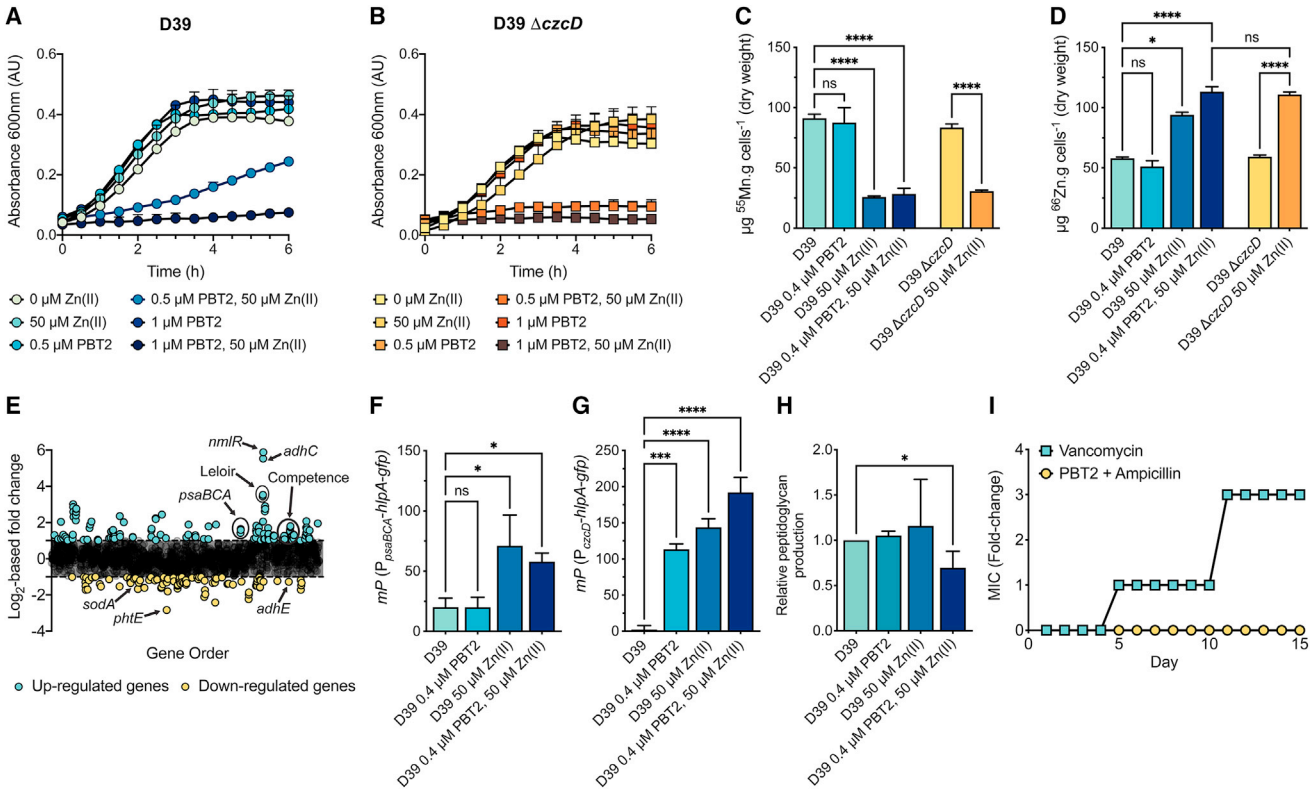


**Figure 2. PBT2 + Zn dysregulates *S. pneumoniae* metal homeostasis**

(A and B) Phenotypic impact of Zn, PBT2, and PBT2 + Zn on *S. pneumoniae* D39 (A) and D39 Δ*czcD* (B) growth in cation-defined growth medium (CDM) supplemented as indicated. The data correspond with mean (± standard error of the mean) absorbance 600 nm measurements from three independent biological experiments. Error bars, where not visible, are overlapped by the representative symbols.

(C and D) Whole cell metal ion accumulation of Mn (C) and Zn (D) in the *S. pneumoniae* strains D39 and D39 Δ*czcD* in the presence of Zn, PBT2, and PBT2+Zn grown in CDM. Error bars indicate standard deviation of the mean from three biological replicates, ns = $p > 0.05$, * = $p < 0.05$, **** = $p < 0.0001$, one-way analysis of variance with the Tukey post-test.

(E) RNA sequencing of *S. pneumoniae* D39 Δ*czcD* to determine relative gene expression of Zn-treated cultures compared to untreated, expressed as $\log_2$-fold change. Each dot represents a gene, distributed on the x axis in accordance with locus tag numbering for D39. Genes more highly expressed in the presence of 100 μM $ZnSO_4$ are present above the x axis (blue), with those below the x axis expressed at a lower level (yellow). Genes of interest are annotated with their putative or characterized functions.

(F and G) Fluorescence polarization assays conducted using *S. pneumoniae* $P_{psaBCA}$-*hlpA-gfp* (F) and $P_{czcD}$-*hlpA-gfp* (G). The data correspond to mean (± standard deviation) mid-log *mP* measurements from three biological replicates. Statistical significance was determined by one-way analysis of variance with the Tukey post-test, ns = $p > 0.05$, * = $p < 0.05$, *** = $p < 0.001$, **** = $p < 0.0001$.

(H) Relative quantitation of total cellular peptidoglycan levels from *S. pneumoniae* D39 grown in CDM supplemented as indicated. Data represent the mean (± standard deviation) of three independent biological experiments. Statistical significance was determined by a two-tailed unpaired *t* test, * = $p < 0.05$.

(I) Development of resistance assays for *S. pneumoniae* D39 during serial passage in the presence of sub-inhibitory concentrations of PBT2 + ampicillin or vancomycin, as a positive control, in cation-adjusted Mueller-Hinton broth (CA-MHB). Experiment was terminated at 15 days owing to loss of viability in the presence of PBT2 + ampicillin. Data represent three biological replicates.

encoding a fluorescent reporter regulated by SczA (the Zn-dependent metalloregulator that dictates *czcD* expression) showed an increase in cellular fluorescence in response to PBT2, Zn, and PBT2 + Zn, indicating transcriptional activation of *czcD* expression (Figure 2G). Consistent with the whole cell metal accumulation analyses, PBT2 + Zn treatment induced the greatest level of fluorophore expression. Building on these observations, which showed that PBT2 + Zn enhanced Zn accumulation in the wild-type strain, we investigated whether peptidoglycan abundance was impacted in PBT2 + Zn-treated cells as a proxy for measurement of GlmU activity. Peptidoglycan levels were reduced in *S. pneumoniae* D39 in PBT2 + Zn-treated cells, relative to untreated cells (Figure 2H), and cell morphology altered (Figures S3E–S3H). We then investigated the potential for *S. pneumoniae* to develop resistance to ampicillin in the presence of PBT2. Resistant mutants were unable to be isolated during serial passage over a period of 15 days in the presence of PBT2, after which the bacteria were no longer viable (Figure 2I). We next investigated the susceptibility of multidrug-resistant *S. pneumoniae* treated with PBT2 + Zn to antibiotics.

This was addressed using the *S. pneumoniae* Spain23F ST81 strain (23F), which harbors penicillin, ampicillin, chloramphenicol, and tetracycline resistance determinants (Croucher et al., 2009). Treatment with PBT2 + Zn elicited broad transcriptomic,

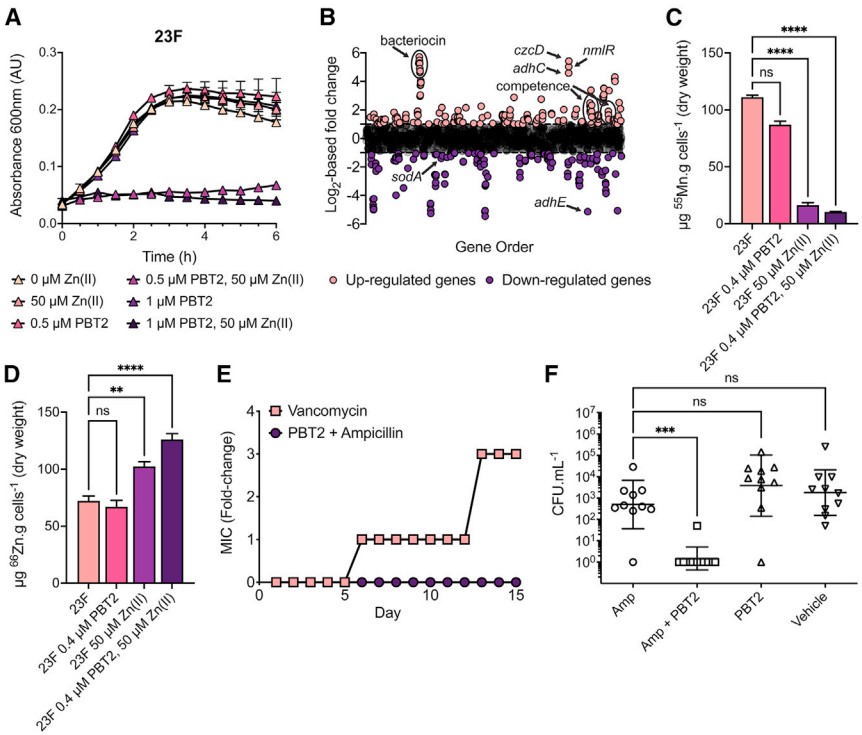


**Figure 3. PBT2 + Zn disrupts metal homeostasis in multidrug-resistant *S. pneumoniae* and breaks *in vivo* ampicillin resistance**

(A) Phenotypic impact of Zn, PBT2, and PBT2 + Zn on *S. pneumoniae* 23F growth in cation-adjusted Mueller-Hinton broth (CA-MHB) supplemented as indicated. The data correspond with the mean (± standard error of the mean) absorbance 600 nm measurements from three independent biological experiments. Error bars, where not visible, are overlapped by the representative symbols.

(B) RNA sequencing of *S. pneumoniae* 23F to determine relative gene expression, expressed as $log_2$-fold change. Each dot represents a gene, distributed on the x axis in accordance with locus tag numbering for 23F. Genes more highly expressed in the presence of 8 μM PBT2 + 32 μM $ZnSO_4$ are present above the x axis (pink), with those below the x axis expressed at a lower level (purple). Genes of interest are annotated with their putative or characterized functions.

(C and D) Whole cell metal ion accumulation of Mn (C) and Zn (D) in *S. pneumoniae* 23F in the presence of PBT2, Zn, and PBT2 + Zn grown in CA-MHB. Error bars indicate standard deviation of the mean from three biological replicates, ns = $p > 0.05$, ** = $p < 0.01$, **** = $p < 0.0001$, one-way analysis of variance with the Tukey post-test.

(E) Development of resistance assays for *S. pneumoniae* 23F during serial passage in the presence of sub-inhibitory concentrations of PBT2 + ampicillin or vancomycin, as a positive control, in CA-MHB. Experiment was terminated at 15 days owing to a loss of viability in the presence of PBT2 + ampicillin. Data represent three biological replicates.

(F) Enumeration of colony-forming units (CFUs) of *S. pneumoniae* from the lungs of BALB/c mice, following intranasal challenge with $5 \times 10^5$ CFU of strain DAW30 (n = 10). Colonization was examined at 24 h after the challenge. BALB/c mice were treated with combinations of ampicillin, PBT2, ampicillin + PBT2 or vehicle at 0 h and 6 h after infection via oral gavage (PBT2, vehicle) and/or subcutaneous ampicillin. Data represent the mean (± standard deviation) of two independent experiments with statistical analyses performed by the Mann-Whitney *U* test. ns = $p > 0.05$, *** = $p = 0.001$.

phenotypic, morphological, and metal dysregulatory impacts in *S. pneumoniae* 23F, consistent with observations from the D39 strains (Figures 3A–3D, S4A–S4H, Table S4). Given the pleiotropic impacts of Zn intoxication on bacterial protein function and cell morphology, the rescue of other β-lactams and other classes of clinically relevant antibiotics was examined. Minimum inhibitory concentration determinations were performed using sub-inhibitory combinations of PBT2 + Zn (Table S5) in combination with penicillin, ampicillin, chloramphenicol, and tetracycline at antibiotic concentrations that did not affect bacterial survival (Table 2). Upon treatment with PBT2 + Zn, *S. pneumoniae* 23F displayed significantly reduced survival to penicillin ($p < 0.01$, two-tailed unpaired *t* test), ampicillin ($p < 0.01$, two-tailed unpaired *t* test), chloramphenicol ($p < 0.01$, two-tailed unpaired *t* test) and tetracycline ($p < 0.01$, two-tailed unpaired *t* test) (Figures S4I–S4L, Table 2). Next, we investigated the potential for *S. pneumoniae* 23F to develop resistance to ampicillin in the presence of PBT2. As for *S. pneumoniae* D39, no resistant mutants were isolated during serial passage in the presence of PBT2 before the loss of bacterial viability (Figure 3E).

During lung infection, this niche naturally increases in Zn abundance (Eijkelkamp et al., 2019; McDevitt et al., 2011). Therefore, we investigated the therapeutic potential of the ionophore PBT2 in combination with ampicillin, without the addition of exogenous Zn. The ampicillin-resistant *S. pneumoniae* DAW30 serotype 6 strain, which is capable of mediating murine lung infection, was used to investigate the efficacy of PBT2 + ampicillin treatment in BALB/c mice, because the multidrug-resistant capsular serotype 23 strain has a poor capacity for virulence in murine models of infection (Briles et al., 1992, 2003). As for *S. pneumoniae* 23F, *S. pneumoniae* DAW30 ampicillin resistance was broken by the addition of PBT2 + Zn (Table 2). The *S. pneumoniae* DAW30 strain was used to investigate PBT2 + ampicillin treatment in a lung infection model, which revealed that PBT2 treatment alone had no therapeutic effect, while treatment with ampicillin alone provided some therapeutic benefit (Figure 3F). The combination of PBT2 + ampicillin significantly improved treatment outcomes and substantially decreased the bacterial burden in the lungs, consistent with the host modulation of Zn within this niche as a component of the innate immune response to infection (Figure 3F). Taken together, these data indicate that host modulation of Zn abundance is necessary and sufficient for PBT2-mediated amplification of antibiotic potency. Further, the breakage of antibiotic resistance *in vivo* has broad relevance for the treatment of pneumonia caused by resistant *S. pneumoniae* strains.

## DISCUSSION

The efficacy of frontline treatments for CABP, of which *S. pneumoniae* remains the primary cause, have been challenged by

**Table 2. Combination of PBT2 and Zn resensitizes pathogenic *S. pneumoniae* strains to antibiotics of various classes**

| | MIC (μg.mL$^{-1}$)[b] | | | | | | | |
|---|---|---|---|---|---|---|---|---|
| | 23F | | | | DAW30 | | | |
| | PBT2: 0 μM | PBT2: 8 μM | | | PBT2: 0 μM | PBT2: 8 μM | | |
| Antibiotic | Zn: 0 μM | Zn: 32 μM | PBT2: 8 μM | Zn: 32 μM | Zn: 0 μM | Zn: 32 μM | PBT2: 8 μM | Zn: 32 μM |
| Penicillin[a] | 2 | 0.5 | 2 | 2 | 4 | <0.062* | 4 | 4 |
| Ampicillin | 8 | 0.5* | 8 | 8 | 4 | <0.062* | 4 | 4 |
| Chloramphenicol | 16 | 2* | 16 | 16 | 4 | 0.125* | 8 | 8 |
| Tetracycline | 32 | 1* | 32 | 32 | <0.062 | <0.062 | <0.062 | <0.062 |

Minimum inhibitory concentration (MIC) values were determined by broth microdilution according to Clinical and Laboratory Standards Institute (2017) guidelines, n = 3.

[a]MIC for non-meningitis infection.

[b]Antibiotic MICs that have changed from resistant to sensitive in the presence of PBT2 + Zn are denoted by asterisk designation.

increasing rates of multidrug-resistance in combination with escape from vaccine prophylaxis. Although antibiotics such as vancomycin, linezolid, and tigecycline remain efficacious, these are predominantly restricted for use in clinical settings and have more complex treatment regimens to minimize potential adverse effects (Sader et al., 2019; Zhang et al., 2019). Increased reliance on last-line antibiotics is also likely to lead to selection for resistance, with increasing rates of non-susceptible tigecycline isolates being reported (Sader et al., 2019; Zhang et al., 2019). Further complicating this landscape is the challenge in achieving effective clinical intervention against multidrug-resistant *S. pneumoniae* isolates, which occurs in 30% of United States isolates and 46% of mainland China isolates (Kim et al., 2016; Wang et al., 2019). Mortality rates from severe pneumonia owing to treatment failure range between 2.4% and 31% (≤72 h of hospitalization) and 3.9% and 11% (>72 h of hospitalization) (Garcia-Vidal and Carratala, 2009; Oster et al., 2013).

Developing strategies to overcome multidrug resistance in bacterial pathogens is a global priority. Here, our data revealed that *S. pneumoniae* Zn stress impacts numerous essential cellular processes, notably central carbon metabolism and peptidoglycan biosynthesis, that are vital for infection (van Opijnen and Camilli, 2012). Zn intoxication in *S. pneumoniae* manifested as a reduction in resistance to various antibiotic classes. This suggested that the antimicrobial activity of exogenous Zn could also be harnessed to potentiate the efficacy of antibiotic treatment. In the context of pneumococcal infection, it has been established that the innate immune response manipulates the chemistry of niches such as the lungs (Eijkelkamp et al., 2019; McDevitt et al., 2011) and exploits the antimicrobial activity of Zn. Here, we showed that the antimicrobial activity of exogenous Zn could be potentiated by PBT2 to decrease or break antibiotic resistance in *S. pneumoniae* strains. This finding builds on recent observations from Gram-negative bacterial pathogens wherein PBT2 has been shown to break antibiotic resistance, although the molecular basis of PBT2 action has been attributed by inference (Bohlmann et al., 2018; De Oliveira et al., 2020; Harbison-Price et al., 2020; Jen et al., 2020). Distinct from those works, our data establish that the molecular basis for PBT2 potentiation of antibiotic efficacy arises from the dysregulation of bacterial metal ion homeostasis and the disruption of essential cellular processes. In GlmU, the presence of a surface-exposed adventitious metal-binding site renders the protein susceptible to Zn-mediated perturbation of activity. Under normal physiological conditions, the pneumococcal Zn homeostatic machinery tightly regulates intracellular Zn abundance (Kloosterman et al., 2007; Plumptre et al., 2014), preventing the perturbation of GlmU activity. This obviates selection pressure on naturally occurring, adventitious Zn-binding sites that are broadly distributed throughout the pneumococcal proteome [approximately 8% of proteins (Neville et al., 2020; Sun et al., 2011)] and exemplified by GlmU. The intrinsic Zn resistance mechanisms of *S. pneumoniae* can be rapidly overwhelmed by PBT2 mediated Zn influx, resulting in the inappropriate interaction of Zn with GlmU and other susceptible proteins. However, we note that the impact of PBT2 + Zn in perturbing GlmU activity *in vivo* is inferred, as the ionic interaction of Zn with this intracellular bacterial protein precludes direct capture and measurement. Nevertheless, the modality of PBT2 action seems to be consistent with an amplification of the antimicrobial effect of Zn within the lungs (Eijkelkamp et al., 2019; McDevitt et al., 2011), leading to an increased susceptibility of *S. pneumoniae* to low-cost, frontline antibiotics such as ampicillin, while the multitude of cellular disruptions mediated by Zn seem to preclude the evolution of resistance.

There are several important caveats with respect to this study that should be noted. Despite the efficacy of PBT2 in combination with β-lactam antibiotics against clinical *S. pneumoniae* strains, formal pharmacokinetic, pharmacodynamic, and toxicity assessments of the combination treatment have not yet been performed. Further, *in vivo* testing was limited to non-randomized murine models of infection, and so, the therapeutic potential of PBT2 + ampicillin cannot be fully established until appropriate safety and efficacy trials are performed in humans.

Repurposing existing drugs such as PBT2 represents a viable alternative to *de novo* drug discovery owing to the benefits of decreased time, cost, and risks by comparison with drug innovation (Chong and Sullivan, 2007). During the phase II human trial of PBT2, no clinically significant changes in plasma Cu, Fe, or Zn concentrations were observed (Bush, 2013; Huntington Study Group Reach, 2015; Lannfelt et al., 2008; Villemagne et al., 2017). This indicates that PBT2 does not dysregulate metal ion homeostasis in humans, consistent with the fundamental differences in metal ion homeostatic mechanisms between prokaryotes and higher order

eukaryotes. The capacity of PBT2 to rescue the efficacy of frontline antibiotics against multidrug-resistant *S. pneumoniae* serotypes provides a novel antimicrobial stewardship pathway to overcome drug resistance. This approach has the potential to preserve new, high-cost antimicrobials, such as lefamulin, and other last-line antibiotics for use in complex and/or critical care scenarios. This study highlights the potential for PBT2 to be used in combination with existing antibiotics as a low-cost adjunct to break drug resistance and restore the efficacy of frontline antibiotics for the treatment of severe bacterial pneumonia infections.

## STAR★METHODS

Detailed methods are provided in the online version of this paper and include the following:

- KEY RESOURCES TABLE
- RESOURCE AVAILABILITY
  - Lead contact
  - Materials availability
  - Data and code availability
- EXPERIMENTAL MODEL AND SUBJECT DETAILS
  - Bacterial strains and growth
  - Animal models
- METHOD DETAILS
  - Bacterial growth
  - Minimum inhibitory concentration (MIC) determination and survival studies
  - Whole cell metal accumulation
  - Antibiotic survival
  - Development of resistance analyses
  - RNA sequencing and qRT-PCR
  - Metabolomic sample preparation
  - GlmM and GlmU expression and purification
  - GlmM and GlmU enzyme activity assays
  - Metal content analysis of GlmU proteins
  - GlmU crystallization, data collection, structure solution and refinement
  - GlmU residue conservation analysis
  - Scanning electron microscopy (SEM)
  - Peptidoglycan detection assay
  - Fluorescence polarization assay
  - Murine challenge experiments
  - Ethics statement
- QUANTIFICATION AND STATISTICAL ANALYSIS

## SUPPLEMENTAL INFORMATION

Supplemental information can be found online at https://doi.org/10.1016/j.celrep.2021.110202.

## ACKNOWLEDGMENTS

This work was supported by the National Health and Medical Research Council (NHMRC) Project Grants 1080784 and 1140554 to C.A.M. and M.J.M., 1176180 and 1194130 to M.J.W., 1071659 to M.J.W. and M.V.I., and 1122582 to C.A.M. and the Australian Research Council (ARC) Discovery Project Grant DP170102102 to C.A.M. This work was also supported by the National Institutes of Health grants (1U01AI124302 and 1RO1AI110618) to J.W.R. S.L.N. is an NHMRC Early Career Research Fellow (1142695) and C.A.M. and M.J.M. are ARC Future Fellows (FT170100006 and FT180100397, respectively). Part of this study was carried out using the MX2 beamline at the Australian Synchrotron, which is part of Australian Nuclear Science and Technology Organization (ANSTO) and made use of the Australian Cancer Research Foundation (ACRF) Detector. We thank the beamline staff for their enthusiastic and professional support, Prof. Jan-Willem Veening (University of Lausanne) for provision of the *hlpA* fluorescent construct and Prof. Michael Caparon (Washington University) for the pABG5-3 mini plasmid.

## AUTHOR CONTRIBUTIONS

E.B.B., A.T., S.L.N., B.A.C., D.M.P.D.O., B.K., A.G.M., M.J.M., M.J.W., J.R.W., and C.A.M. conceived and designed experiments. E.B.B., A.T., S.L.N., A.R.I., L.B., B.A.E., J.W.R., and C.A.M. undertook antimicrobial sensitivity testing. E.B.B. and D.M.P.D.O. investigated resistance development. E.B.B., A.T., S.L.N., A.R.I., B.A.C., D.M.P.D.O., B.K., L.B., K.G., B.A.E., M.J.W., J.W.R., and C.A.M. conducted mechanism of action and heavy metal homeostasis studies. E.B.B., S.L.N., A.R.I., B.A.E., and J.W.R. undertook work using murine models of infection. M.S., S.R.U., K.G., and M.J.M. performed the structural and biochemical studies of GlmM and GlmU. I.M.E.-D. and M.V.I. provided essential reagents. M.J.M., M.J.W., J.R.W., and C.A.M. supervised the research. C.A.M. wrote the manuscript. E.B.B., A.T., S.L.N., D.M.P.D.O., A.G.M., M.J.M., M.J.W., J.R.W., and C.A.M. edited and reviewed the manuscript. All authors approved the final manuscript.

## DECLARATION OF INTERESTS

C.A.M., A.G.M., M.V.I., and M.J.W. hold an intellectual property interest in this work (PCT/AU2018/051116).

## INCLUSION AND DIVERSITY

One or more of the authors of this paper self-identifies as an underrepresented ethnic minority in science. One or more of the authors of this paper self-identifies as living with a disability.

Received: January 6, 2021
Revised: September 24, 2021
Accepted: December 13, 2021
Published: January 11, 2022

## REFERENCES

Amin, A.N., Cerceo, E.A., Deitelzweig, S.B., Pile, J.C., Rosenberg, D.J., and Sherman, B.M. (2014). The hospitalist perspective on treatment of community-acquired bacterial pneumonia. Postgrad. Med. *126*, 18–29.

Anders, S., and Huber, W. (2010). Differential expression analysis for sequence count data. Nat. Preced. https://doi.org/10.1038/npre.2010.4282.2.

Basnayake, T.L., Morgan, L.C., and Chang, A.B. (2017). The global burden of respiratory infections in indigenous children and adults: a review. Respirology *22*, 1518–1528.

Begg, S.L., Eijkelkamp, B.A., Luo, Z., Couñago, R.M., Morey, J.R., Maher, M.J., Ong, C.L., McEwan, A.G., Kobe, B., O'Mara, M.L., et al. (2015). Dysregulation of transition metal ion homeostasis is the molecular basis for cadmium toxicity in *Streptococcus pneumoniae*. Nat. Commun. *6*, 6418.

Bohlmann, L., De Oliveira, D.M.P., El-Deeb, I.M., Brazel, E.B., Harbison-Price, N., Ong, C.Y., Rivera-Hernandez, T., Ferguson, S.A., Cork, A.J., Phan, M.D., et al. (2018). Chemical synergy between ionophore PBT2 and zinc reverses antibiotic resistance. mBio *9*, e02391-18.

Bonafede, M.M., Suaya, J.A., Wilson, K.L., Mannino, D.M., and Polsky, D. (2012). Incidence and cost of CAP in a large working-age population. Am. J. Manag. Care *18*, 380–387.

Briles, D.E., Crain, M.J., Gray, B.M., Forman, C., and Yother, J. (1992). Strong association between capsular type and virulence for mice among human isolates of *Streptococcus pneumoniae*. Infect. Immun. *60*, 111–116.

Briles, D.E., Hollingshead, S.K., Paton, J.C., Ades, E.W., Novak, L., van Ginkel, F.W., and Benjamin, W.H., Jr. (2003). Immunizations with pneumococcal surface protein A and pneumolysin are protective against pneumonia in a murine model of pulmonary infection with *Streptococcus pneumoniae*. J. Infect. Dis. *188*, 339–348.

Bush, A.I. (2013). The metal theory of Alzheimer's disease. J. Alzheimers Dis. *33*, S277–S281.

CCP4. (1994). Collaborative computational Project no. 4. Acta Crystallogr. D *D50*, 760–763.

Chen, V.B., Arendall, W.B., 3rd, Headd, J.J., Keedy, D.A., Immormino, R.M., Kapral, G.J., Murray, L.W., Richardson, J.S., and Richardson, D.C. (2010). MolProbity: all-atom structure validation for macromolecular crystallography. Acta Crystallogr. D *66*, 12–21.

Chong, C.R., and Sullivan, D.J. (2007). New uses for old drugs. Nature *448*, 645–646.

Cilloniz, C., Rodriguez-Hurtado, D., and Torres, A. (2018). Characteristics and management of community-acquired pneumonia in the era of global aging. Med. Sci. (Basel). *6*, 35.

Clinical and Laboratory Standards Institute (2017). M100 Performance Standards for Antimicrobial Susceptibility Testing, 27 (Clinical and Laboratory Standards Institute).

Croucher, N.J., Walker, D., Romero, P., Lennard, N., Paterson, G.K., Bason, N.C., Mitchell, A.M., Quail, M.A., Andrew, P.W., Parkhill, J., et al. (2009). Role of conjugative elements in the evolution of the multidrug-resistant pandemic clone *Streptococcus pneumoniae* Spain23F ST81. J. Bacteriol. *191*, 1480–1489.

Davies, M.R., McIntyre, L., Mutreja, A., Lacey, J.A., Lees, J.A., Towers, R.J., Duchêne, S., Smeesters, P.R., Frost, H.R., and Price, D.J. (2019). Atlas of group A streptococcal vaccine candidates compiled using large-scale comparative genomics. Nat. Genet. *51*, 1035–1043.

De Oliveira, D.M.P., Bohlmann, L., Conroy, T., Jen, F.E., Everest-Dass, A., Hansford, K.A., Bolisetti, R., El-Deeb, I.M., Forde, B.M., Phan, M.D., et al. (2020). Repurposing a neurodegenerative disease drug to treat Gram-negative antibiotic-resistant bacterial sepsis. Sci. Transl. Med. *12*, eabb3791.

Eijkelkamp, B.A., Morey, J.R., Neville, S.L., Tan, A., Pederick, V.G., Cole, N., Singh, P.P., Ong, C.Y., Gonzalez de Vega, R., Clases, D., et al. (2019). Dietary zinc and the control of *Streptococcus pneumoniae* infection. PLoS Pathog. *15*, e1007957.

Emsley, P., and Cowtan, K. (2004). Coot: model-building tools for molecular graphics. Acta Crystallogr. D *60*, 2126–2132.

Evans, P.R., and Murshudov, G.N. (2013). How good are my data and what is the resolution? Acta Crystallogr. D *69*, 1204–1214.

Garcia-Vidal, C., and Carratala, J. (2009). Early and late treatment failure in community-acquired pneumonia. Semin. Respir. Crit. Care Med. *30*, 154–160.

Gladstone, R.A., Lo, S.W., Lees, J.A., Croucher, N.J., Van Tonder, A.J., Corander, J., Page, A.J., Marttinen, P., Bentley, L.J., and Ochoa, T.J. (2019). International genomic definition of pneumococcal lineages, to contextualise disease, antibiotic resistance and vaccine impact. EBioMedicine. *43*, 338–346.

Haase, H., and Rink, L. (2014). Multiple impacts of zinc on immune function. Metallomics *6*, 1175–1180.

Hadžija, O. (1974). A simple method for the quantitative determination of muramic acid. Anal. Biochem. *60*, 512–517.

Harbison-Price, N., Ferguson, S.A., Heikal, A., Taiaroa, G., Hards, K., Nakatani, Y., Rennison, D., Brimble, M.A., El-Deeb, I.M., Bohlmann, L., et al. (2020). Multiple bactericidal mechanisms of the zinc ionophore PBT2. mSphere. *5*, e00157-20.

Hayes, A., Lacey, J.A., Morris, J.M., Davies, M.R., and Tong, S.Y.C. (2020). Restricted sequence variation in *Streptococcus pyogenes* penicillin binding proteins. mSphere *5*, e00090-20.

Huntington Study Group Reach, H.D.I. (2015). Safety, tolerability, and efficacy of PBT2 in Huntington's disease: a phase 2, randomised, double-blind, placebo-controlled trial. Lancet Neurol. *14*, 39–47.

Jen, F.E., Everest-Dass, A.V., El-Deeb, I.M., Singh, S., Haselhorst, T., Walker, M.J., von Itzstein, M., and Jennings, M.P. (2020). *Neisseria gonorrhoeae* becomes susceptible to polymyxin B and colistin in the presence of PBT2. ACS Infect. Dis. *6*, 50–55.

Kabsch, W. (2010). Xds. Acta Crystallogr. D *66*, 125–132.

Kearse, M., Moir, R., Wilson, A., Stones-Havas, S., Cheung, M., Sturrock, S., Buxton, S., Cooper, A., Markowitz, S., and Duran, C. (2012). Geneious Basic: an integrated and extendable desktop software platform for the organization and analysis of sequence data. Bioinformatics *28*, 1647–1649.

Kim, L., McGee, L., Tomczyk, S., and Beall, B. (2016). Biological and epidemiological features of antibiotic-resistant *Streptococcus pneumoniae* in pre- and post-conjugate vaccine eras: a United States perspective. Clin. Microbiol. Rev. *29*, 525–552.

Kjos, M., Aprianto, R., Fernandes, V.E., Andrew, P.W., van Strijp, J.A., Nijland, R., and Veening, J.W. (2015). Bright fluorescent *Streptococcus pneumoniae* for live-cell imaging of host-pathogen interactions. J. Bacteriol. *197*, 807–818.

Kjos, M., and Veening, J.W. (2014). Tracking of chromosome dynamics in live *Streptococcus pneumoniae* reveals that transcription promotes chromosome segregation. Mol. Microbiol. *91*, 1088–1105.

Kloosterman, T.G., van der Kooi-Pol, M.M., Bijlsma, J.J., and Kuipers, O.P. (2007). The novel transcriptional regulator SczA mediates protection against Zn2+ stress by activation of the Zn2+-resistance gene *czcD* in *Streptococcus pneumoniae*. Mol. Microbiol. *65*, 1049–1063.

Kostrewa, D., D'Arcy, A., Takacs, B., and Kamber, M. (2001). Crystal structures of *Streptococcus pneumoniae* N-acetylglucosamine-1-phosphate uridyltransferase, GlmU, in apo form at 2.33 Å resolution and in complex with UDP-N-acetylglucosamine and Mg(2+) at 1.96 A resolution. J. Mol. Biol. *305*, 279–289.

Lacks, S., and Hotchkiss, R.D. (1960). A study of the genetic material determining an enzyme in Pneumococcus. Biochim. Biophys. Acta. *39*, 508–518.

Langmead, B., and Salzberg, S.L. (2012). Fast gapped-read alignment with Bowtie 2. Nat. Methods *9*, 357.

Lannfelt, L., Blennow, K., Zetterberg, H., Batsman, S., Ames, D., Harrison, J., Masters, C.L., Targum, S., Bush, A.I., Murdoch, R., et al. (2008). Safety, efficacy, and biomarker findings of PBT2 in targeting Abeta as a modifying therapy for Alzheimer's disease: a phase IIa, double-blind, randomised, placebo-controlled trial. Lancet Neurol. *7*, 779–786.

Li, H., Handsaker, B., Wysoker, A., Fennell, T., Ruan, J., Homer, N., Marth, G., Abecasis, G., and Durbin, R. (2009). The sequence alignment/map format and SAMtools. Bioinformatics *25*, 2078–2079.

Li, S., Kang, J., Yu, W., Zhou, Y., Zhang, W., Xin, Y., and Ma, Y. (2012). Identification of *M. tuberculosis* Rv3441c and *M. smegmatis* MSMEG_1556 and essentiality of *M. smegmatis* MSMEG_1556. PLoS One *7*, e42769.

Li, Y., Zhou, Y., Ma, Y., and Li, X. (2011). Design and synthesis of novel cell wall inhibitors of *Mycobacterium tuberculosis* GlmM and GlmU. Carbohydr. Res. *346*, 1714–1720.

Ling, L.L., Schneider, T., Peoples, A.J., Spoering, A.L., Engels, I., Conlon, B.P., Mueller, A., Schaberle, T.F., Hughes, D.E., Epstein, S., et al. (2015). A new antibiotic kills pathogens without detectable resistance. Nature *520*, 388.

McCoy, A.J., Grosse-Kunstleve, R.W., Adams, P.D., Winn, M.D., Storoni, L.C., and Read, R.J. (2007). Phaser crystallographic software. J. Appl. Crystallogr. *40*, 658–674.

McDevitt, C.A., Ogunniyi, A.D., Valkov, E., Lawrence, M.C., Kobe, B., McEwan, A.G., and Paton, J.C. (2011). A molecular mechanism for bacterial susceptibility to zinc. PLoS Pathog. *7*, e1002357.

McKinnell, J.C.P., Blumberg, P., Murty, S., and Tillotson, G. (2017). Clinical predictors of antibiotic failure in adult outpatients with community-acquired pneumonia. Am. J. Respir. Crit. Care Med. *195*, A2644.

Murshudov, G.N., Skubak, P., Lebedev, A.A., Pannu, N.S., Steiner, R.A., Nicholls, R.A., Winn, M.D., Long, F., and Vagin, A.A. (2011). REFMAC5 for the refinement of macromolecular crystal structures. Acta Crystallogr. D *67*, 355–367.

Neville, S.L., Eijkelkamp, B.A., Lothian, A., Paton, J.C., Roberts, B.R., Rosch, J.W., and McDevitt, C.A. (2020). Cadmium stress dictates central carbon flux and alters membrane composition in *Streptococcus pneumoniae*. Commun. Biol. *3*, 694.

O'Grady, K.F., Hall, K., Bell, A., Chang, A.B., and Potter, C. (2018). Review of respiratory diseases among aboriginal and Torres Strait islander children. Aust. Indigenous Health Bull. *18*, 1–32.

Oster, G., Berger, A., Edelsberg, J., and Weber, D.J. (2013). Initial treatment failure in non-ICU community-acquired pneumonia: risk factors and association with length of stay, total hospital charges, and mortality. J. Med. Econ. *16*, 809–819.

Pettersen, E.F., Goddard, T.D., Huang, C.C., Couch, G.S., Greenblatt, D.M., Meng, E.C., and Ferrin, T.E. (2004). UCSF Chimera—a visualization system for exploratory research and analysis. J. Comput. Chem. *25*, 1605–1612.

Peyrani, P., Mandell, L., Torres, A., and Tillotson, G.S. (2019). The burden of community-acquired bacterial pneumonia in the era of antibiotic resistance. Expert Rev. Respir. Med. *13*, 139–152.

Plumptre, C.D., Eijkelkamp, B.A., Morey, J.R., Behr, F., Couñago, R.M., Ogunniyi, A.D., Kobe, B., O'Mara, M.L., Paton, J.C., and McDevitt, C.A. (2014). AdcA and AdcAII employ distinct zinc acquisition mechanisms and contribute additively to zinc homeostasis in *Streptococcus pneumoniae*. Mol. Microbiol. *91*, 834–851.

Polsky, D., Bonafede, M., and Suaya, J.A. (2012). Comorbidities as a driver of the excess costs of community-acquired pneumonia in U.S. commercially-insured working age adults. BMC Health Serv. Res. *12*, 379.

Quinlan, A.R., and Hall, I.M. (2010). BEDTools: a flexible suite of utilities for comparing genomic features. Bioinformatics *26*, 841–842.

Rani, C., and Khan, I.A. (2016). UDP-GlcNAc pathway: potential target for inhibitor discovery against *M. tuberculosis*. Eur. J. Pharm. Sci. *83*, 62–70.

Sader, H.S., Mendes, R.E., Le, J., Denys, G., Flamm, R.K., and Jones, R.N. (2019). Antimicrobial susceptibility of *Streptococcus pneumoniae* from North America, Europe, Latin America, and the asia-Pacific region: results from 20 years of the SENTRY antimicrobial surveillance program (1997-2016). Open Forum Infect. Dis. *6*, S14–S23.

Souvorov, A., Agarwala, R., and Lipman, D.J. (2018). SKESA: strategic k-mer extension for scrupulous assemblies. Genome Biol. *19*, 153.

Strand, T.A., Briles, D.E., Gjessing, H.K., Maage, A., Bhan, M.K., and Sommerfelt, H. (2001). Pneumococcal pulmonary infection, septicaemia and survival in young zinc-depleted mice. Br. J. Nutr. *86*, 301–306.

Strand, T.A., Hollingshead, S.K., Julshamn, K., Briles, D.E., Blomberg, B., and Sommerfelt, H. (2003). Effects of zinc deficiency and pneumococcal surface protein a immunization on zinc status and the risk of severe infection in mice. Infect. Immun. *71*, 2009–2013.

Sulzenbacher, G., Gal, L., Peneff, C., Fassy, F., and Bourne, Y. (2001). Crystal structure of *Streptococcus pneumoniae* N-acetylglucosamine-1-phosphate uridyltransferase bound to acetyl-coenzyme A reveals a novel active site architecture. J. Biol. Chem. *276*, 11844–11851.

Sun, X., Xiao, C.L., Ge, R., Yin, X., Li, H., Li, N., Yang, X., Zhu, Y., He, X., and He, Q.Y. (2011). Putative copper- and zinc-binding motifs in *Streptococcus pneumoniae* identified by immobilized metal affinity chromatography and mass spectrometry. Proteomics *11*, 3288–3298.

van Opijnen, T., and Camilli, A. (2012). A fine scale phenotype-genotype virulence map of a bacterial pathogen. Genome Res. *22*, 2541–2551.

Villemagne, V.L., Rowe, C.C., Barnham, K.J., Cherny, R., Woodward, M., Bozinosvski, S., Salvado, O., Bourgeat, P., Perez, K., Fowler, C., et al. (2017). A randomized, exploratory molecular imaging study targeting amyloid beta with a novel 8-OH quinoline in Alzheimer's disease: the PBT2-204 IMAGINE study. Alzheimers Dement. *3*, 622–635.

Wang, C.Y., Chen, Y.H., Fang, C., Zhou, M.M., Xu, H.M., Jing, C.M., Deng, H.L., Cai, H.J., Jia, K., Han, S.Z., et al. (2019). Antibiotic resistance profiles and multidrug resistance patterns of *Streptococcus pneumoniae* in pediatrics: a multicenter retrospective study in mainland China. Medicine (Baltimore) *98*, e15942.

World Health Organization (2003). Pneumococcal vaccines - WHO position paper. WER *78* (*14*), 110–119.

World Health Organization (2010). Treatment and prevention of pneumonia. In Sixty-third World Health Assembly, World Health Organization., ed. (Geneva: World Health Organization), pp. 1–4, A63/26.

Zhang, Z., Chen, M., Yu, Y., Pan, S., and Liu, Y. (2019). Antimicrobial susceptibility among *Streptococcus pneumoniae* and *Haemophilus influenzae* collected globally between 2015 and 2017 as part of the Tigecycline Evaluation and Surveillance Trial (TEST). Infect. Drug Resist. *12*, 1209–1220.

Zhou, Y., Xin, Y., Sha, S., and Ma, Y. (2011). Kinetic properties of *Mycobacterium tuberculosis* bifunctional GlmU. Arch. Microbiol. *193*, 751–757.

## STAR★METHODS

### KEY RESOURCES TABLE

| REAGENT or RESOURCE | SOURCE | IDENTIFIER |
|---|---|---|
| **Bacterial and virus strains** | | |
| *S. pneumoniae* D39; capsular serotype 2 strain | National Collection of Type Cultures | NCTC7466 |
| *S. pneumoniae* D39 Δ*czcD::ery*$^R$ | (Begg et al., 2015) | N/A |
| *S. pneumoniae* Spain23F; ATCC 700669 multi-drug resistant Spain 23F ST81 lineage | (Croucher et al., 2009) | N/A |
| *S. pneumoniae* DAW30; capsular serotype 6 clinical isolate | This paper | N/A |
| *S. pneumoniae* D39 *hlpA_hlpA-rfp*_Cam$^R$ | (Kjos and Veening, 2014) | MK119 |
| *S. pneumoniae* D39 *hlpA_hlpA-rfp*_Cam$^R$ Δ*spd_1789*::(P$_{czcD}$-*hlpA-gfp*_Spec$^R$) | This paper | BAC100 |
| *S. pneumoniae* D39 *hlpA_hlpA-rfp*_Cam$^R$ Δ*spd_1789*::(P$_{psaBCA}$-*hlpA-gfp*_Spec$^R$) | This paper | BAC101 |
| *Escherichia coli* BL21(DE3); *fhuA2 [lon] ompT gal (λ DE3) [dcm] ΔhsdS* | New England Biolabs | # C2527H |
| **Chemicals, peptides, and recombinant proteins** | | |
| 4-Phenylphenol | Sigma Aldrich | # 134341; CAS 92-69-3 |
| Recombinant, GST-tag cleaved *S. pneumoniae* GlmM | This paper | GlmM |
| Recombinant, GST-tag cleaved *S. pneumoniae* GlmU | This paper | GlmU |
| Recombinant, GST-tag cleaved *S. pneumoniae* GlmU$_{E315AH330A}$ | This paper | GlmU$_{E315AE330A}$ |
| 5,7-dichloro-2-[(dimethylamino)methyl]quinolin-8-ol (PBT2) | (Bohlmann et al., 2018) | PBT2 |
| **Critical commercial assays** | | |
| SuperScript III Platinum SYBR Green One-Step qRT-PCR Kit | ThermoFisher | # 11736059 |
| RNeasy Mini kit | Qiagen | # 74106 |
| NEBuilder HiFi DNA Assembly Master Mix | New England Biolabs | # E2621 |
| **Deposited data** | | |
| D39 RNA sequencing raw and analyzed data | This study | GSE159901 |
| 23F RNA sequencing raw and analyzed data | This study | GSE160372 |
| D39 metabolomics raw and analyzed data | This study | MTBLS318 |
| Zn-bound GlmU structure | This study | 7KR9 |
| **Experimental models: Organisms/strains** | | |
| BALB/cJ | Jackson Laboratory (Bar Harbor, ME) | # 000651 |
| **Oligonucleotides** | | |
| Listed in Table S6 | | N/A |
| **Recombinant DNA** | | |
| pGEX-6p1-GlmM; Expression construct for GlmM | This paper | N/A |
| pGEX-6p1-GlmU; Expression construct for GlmU | This paper | N/A |

(*Continued on next page*)

*Continued*

| REAGENT or RESOURCE | SOURCE | IDENTIFIER |
|---|---|---|
| pGEX-6p1-GlmU$_{E315AH330A}$; Expression construct for GlmU$_{E315AH330A}$ | This paper | N/A |
| Spec$^{R}$; vector with spectinomycin resistance cassette | This paper | pABG5-3 mini |
| **Software and algorithms** | | |
| PRISM | GraphPad | https://www.graphpad.com/scientific-software/prism/ |
| BOWTIE2 v2.2.6 | (Langmead and Salzberg, 2012) | http://bowtie-bio.sourceforge.net/bowtie2/index.shtml |
| SAMtools v1.2 | (Li et al., 2009) | http://samtools.sourceforge.net |
| BEDtools v2.24.0 | (Quinlan and Hall, 2010) | http://code.google.com/p/bedtools |
| R (DESeq Library) v3.2.2 | (Anders and Huber, 2010) | https://www.r-project.org/ |
| shovill v1.0.9 | (Hayes et al., 2020) | https://github.com/tseemann/shovill |
| SKESA v2.3.0 | (Souvorov et al., 2018) | https://github.com/ncbi/SKESA/releases. |
| screen_assembly script | (Davies et al., 2019) | https://github.com/shimbalama/screen_assembly. |
| Geneious Prime v2020.1.2 | (Kearse et al., 2012) | https://www.geneious.com/prime/ |
| UCSF Chimera v1.14.0 | (Pettersen et al., 2004) | https://www.cgl.ucsf.edu/chimera/ |
| REFMAC5 | (Murshudov et al., 2011) | https://www.ccp4.ac.uk/ |
| MOLPROBITY | (Chen et al., 2010) | http://molprobity.biochem.duke.edu/ |
| PHASER | (McCoy et al., 2007) | https://www.ccp4.ac.uk/ |
| AIMLESS | (CCP4, 1994; Evans and Murshudov, 2013) | https://www.ccp4.ac.uk/ |
| XDS | (Kabsch, 2010) | https://xds.mr.mpg.de/ |
| **Other** | | |
| Evactron E50 De-contaminator | XEI Scientific | N/A |
| Q150T Turbomolecular pumped coater | Quorum Tech | N/A |
| JEOI JSM 7100F Scanning electron microscope | JEOL | N/A |
| JEOI JSM 7800F Field emission scanning electron microscope | JEOL | N/A |
| Agilent 8900 Triple Quadrupole ICP-MS | Agilent | N/A |

## RESOURCE AVAILABILITY

### Lead contact

Further information and requests for resources and reagents should be directed to and will be fulfilled by the lead contact, Christopher McDevitt (christopher.mcdevitt@unimelb.edu.au).

### Materials availability

There are restrictions to the availability of the *S. pneumoniae* DAW30 clinical isolate, with requests requiring an MTA with the relevant authority, St. Jude Children's Research Hospital, USA. All other materials generated in this study will be available upon request to Christopher McDevitt.

### Data and code availability

- RNAseq datasets generated and analyzed during the current study are available in the NCBI GEO repository under submission identifiers GSE159901 (D39) and GSE160372 (23F). The metabolomic datasets generated and analyzed during the current study are available in the MetaboLights repository under study identifier MTBLS318. The structure factors and coordinates of the Zn-bound GlmU crystal structure have been deposited in the Protein Data Bank (PDB) with accession code 7KR9.
- This paper does not report original code.
- Any additional information required to reanalyze the data reported in this work paper is available from the lead contact upon request.

## EXPERIMENTAL MODEL AND SUBJECT DETAILS

### Bacterial strains and growth

*S. pneumoniae* D39, Δ*czcD,* 23F and DAW30 were routinely grown in cation-defined media (CDM), which corresponded to C+Y media without supplementation of transition metals (Lacks and Hotchkiss, 1960). The base transition metal concentration of the media was determined by ICP-MS on an Agilent 8900 Triple Quadrupole ICP-MS. All growth experiments were conducted in CDM supplemented with 1 μM $MnSO_4$, with metal ion and PBT2 supplementation where specified. *S. pneumoniae* 23F was grown in cation-adjusted Mueller Hinton II broth (CA-MHB) + 2.5% [v/v] lysed horse blood (LHB) for the Minimum Inhibitory Concentration determination, antibiotic survival studies, and transcriptomic analyses. A concentration of 50% (v/v) lysed horse blood was prepared by dilution of horse blood 1 in 2 into sterile MilliQ water. The horse blood was then subjected to three freeze-thaw cycles from −20°C to room temperature and centrifuged at 7,000 × g for 30 min at 4°C to pellet insoluble material. The supernatant was collected, and the lysed horse blood was stored as 1 ml aliquots at −20°C for up to one month. Cation-adjusted Mueller Hinton II broth was supplemented with 2.5% (v/v) lysed horse blood (CA-MHB+LHB) immediately prior to use. *E. coli* strain BL21 (DE3) (New England BioLabs) was used for protein expression with cultures grown in Luria Broth (LB) at 37°C. *E. coli* strain BL21 (DE3) transformed with plasmid expression constructs were grown in LB supplemented with ampicillin (100 $\mu g.mL^{-1}$) at 37°C.

### Animal models

Female BALB/c mice used in the *in vivo* infection studies were obtained from Jackson laboratory (# 000651) and housed at the animal facility of St Jude Children's Research Hospital,USA. Experiments were conducted on the mice at 8 weeks of age, with all experiments approved under the IACUC protocol number 538-100013-04/12 R1.

## METHOD DETAILS

### Bacterial growth

*S. pneumoniae* strains D39, Δ*czcD*, 23F and DAW30 were grown on Columbia agar plates supplemented with 5% (v/v) horse blood for 18–20 h at 37°C + 5% $CO_2$. Bacteria were collected from blood agar plates with a heat-sterilized inoculation loop, suspended in CDM and adjusted to a final $A_{600}$ of 0.05 in CDM. Bacteria were cultured at 37°C + 5% $CO_2$ until $A_{600}$ of 0.3, centrifuged at 3,273 × *g* for 15 min at 4°C, and resuspended to $A_{600}$ of 0.02 in CDM. $ZnSO_4$ was prepared in MilliQ water at a concentration of 100 mM and sterilized using a 0.2 μm syringe filter. A 5 mM stock solution of PBT2 was prepared by sonication in dimethyl sulfoxide (DMSO) at 50°C for 20 mins and stored at −20°C. For the analysis of growth in the presence of metals and/or PBT2, a 100 μL volume of CDM, with or without $ZnSO_4$, $NiCl_2$, $CuSO_4$, or PBT2.HCl, either singly or in combination, was added at a concentration of two times the test concentration to wells of a 96-well flat bottom plate. A volume of 100 μL CDM, with or without bacteria was added to the appropriate wells with at least two technical replicates and the plate was sealed with a gas-permeable seal (Breathe-Easy, Diversified Biotech). The $A_{600}$ was monitored every 30 mins during incubation of the plate for >6 h at 37°C + 5% $CO_2$, with a brief 100 rpm double orbital shake prior to each reading, using a FLUOstar Omega spectrophotometer (BMG Labtech). Experiments were performed with three biological replicates. The $A_{600}$ was corrected by subtraction of the blank $A_{600}$ using the MARS Data Analysis Software (BMG Labtech) and the blank-corrected data was visualized and analyzed using GraphPad Prism 9.

### Minimum inhibitory concentration (MIC) determination and survival studies

Antibiotic, PBT2 and zinc minimum inhibitory concentrations (MIC) were determined using a slightly modified broth microdilution method. A 5 mM stock solution of PBT2 was prepared by sonication in dimethyl sulfoxide (DMSO) at 50°C for 20 mins and stored at −20°C. $ZnSO_4$ was prepared in MilliQ water at a concentration of 100 mM and sterilized using a 0.2 μm syringe filter. *S. pneumoniae* strains 23F and DAW30 were grown on Columbia agar plates supplemented with 5% (v/v) horse blood for 18–20 h at 37°C + 5% $CO_2$. Bacteria were collected from blood agar plates with a heat-sterilized inoculation loop and suspended in CA-MHB. For MIC analysis of PBT2, bacterial suspensions were diluted to 1 × $10^8$ $CFU.mL^{-1}$ into CA-MHB+LHB, then diluted a further 1 in 100 into CA-MHB+LHB with or without $ZnSO_4$ to a concentration of 1 × $10^6$ $CFU.mL^{-1}$. MIC was analyzed in a 96-well flat bottom plate (Costar). A volume of 50 μL CA-MHB+LHB was transferred to all wells of columns 2-12. CA-MHB+LHB supplemented with PBT2.HCl was added at a volume of 100 μL to column 1 and 50 μL was serially diluted two-fold across the plate to column 11. The bacterial cell suspension was added to the plate at a volume of 50 μL to a final concentration of 5 × $10^5$ $CFU.mL^{-1}$. The plates were sealed with opaque gas-permeable seals (Aeraseal, Sigma Aldrich) and incubated at 37°C for 20 h. The MIC was recorded as the PBT2 concentration of the well displaying no visible growth. For antibiotic MIC analyses, bacterial suspensions were diluted to 1 × $10^8$ $CFU.mL^{-1}$ into CA-MHB+LHB, then diluted a further 1:100 into CA-MHB+LHB with or without $ZnSO_4$, DMSO, or PBT2.HCl, either singly or in combination, to a concentration of 1 × $10^6$ $CFU.mL^{-1}$. The MIC was analyzed in a 96-well flat bottom plate (Costar). A volume of 50 μL CA-MHB+LHB was transferred to all wells of column 2-12. CA-MHB+LHB supplemented with antibiotic was added at a volume of 100 μL to column 1 and 50 μL was serially diluted two-fold across the plate to column 11. The bacterial cell suspension was added to the plate at a volume of 50 μL to a final concentration of 5 × $10^5$ $CFU.mL^{-1}$. The plates were sealed with opaque gas-permeable seals (Aeraseal, Sigma Aldrich) and incubated at 37°C for 20 h. The MIC was recorded as the antibiotic concentration of the well displaying no visible growth. The survival was assessed by determining the colony forming units

(CFU) by 10-fold serial dilutions in 200 μL serum broth and plating 25 μL in technical duplicate spots on blood agar plates. Agar plates were incubated at 37°C + 5% $CO_2$ and the CFU were enumerated after 18–20 h growth. Experiments were performed with three biological replicates.

### Whole cell metal accumulation

Metal content was assessed following growth of *S. pneumoniae* to mid-logarithmic phase ($A_{600}$ = 0.3) in CDM with or without supplementation with metals and/or PBT2.HCl. Stock solutions of $NiCl_2$, $CuSO_4$, and $ZnSO_4$ were prepared at a concentration of 100 mM in MilliQ water and sterilized using a 0.2 μm syringe filter. A 5 mM stock solution of PBT2 was prepared by sonication in DMSO at 50°C for 20 min and stored at −20°C. *S. pneumoniae* strains D39, Δ*czcD*, 23F and DAW30 were grown on Columbia agar plates supplemented with 5% (v/v) horse blood for 18–20 h at 37°C + 5% $CO_2$. Bacteria were collected from blood agar plates with a heat-sterilized inoculation loop, suspended in CDM and adjusted to a final $A_{600}$ of 0.05 in CDM with or without metals and/or PBT2.HCl. For the analyses of PBT2-mediated metal accumulation, concentrations of 50 μM $ZnSO_4$ and 0.4 μM PBT2, were used either singly or in combination. To assess the accumulation of Cu, Ni, and Zn, cultures were supplemented with concentrations of 200 μM $NiCl_2$, 200 μM $CuSO_4$, or 100 μM $ZnSO_4$. At mid-logarithmic phase, the cultures were placed on ice for 5 min and then harvested by centrifugation at 7,000 × *g* for 7 min at 4°C. The bacteria were washed three times with 20 mL chilled PBS supplemented with 5 mM EDTA to remove extracellular metals, followed by three washes with 20 mL chilled PBS to remove residual EDTA. The cell material was transferred to pre-weighed safe-lock microcentrifuge tubes (Eppendorf) using 1 mL of chilled PBS, centrifuged at 21,000 × *g* for 5 min, and the supernatant was removed. The pelleted material was desiccated by incubation of the open tubes at 96°C using a heating block in a fume hood for 18–20 h, followed by resuspension in 35% $HNO_3$ (Seastar Chemicals) and boiling at 96°C for 30 min. Samples were diluted 1:10 in MilliQ water and the metal content was assessed by ICP-MS on an Agilent 8900 Triple Quadrupole ICP-MS. Assays were conducted in biological triplicate and the total metal abundance was determined as the weight (μg) metal per mg of dry cellular material using Microsoft Excel. The data was visualized and analyzed using GraphPad Prism 9. Experiments were performed with three biological replicates.

### Antibiotic survival

*S. pneumoniae* strains D39, Δ*czcD*, and 23F were grown on Columbia agar plates supplemented with 5% (v/v) horse blood for 18–20 h at 37°C + 5% $CO_2$. For the analysis of antibiotic susceptible strains, D39 wild-type and Δ*czcD* bacteria were collected from blood agar plates with a heat-sterilized inoculation loop, suspended in CDM and adjusted to a final $A_{600}$ of 0.05 in CDM. A stock solution of $ZnSO_4$ was prepared at a concentration of 100 mM in MilliQ water and sterilized using a 0.2 μm syringe filter. A stock solution of penicillin G sodium salt was prepared at a concentration of 100 mg.mL$^{-1}$ in MilliQ water and sterilized using a 0.2 μm syringe filter. Bacteria were cultured at 37°C + 5% $CO_2$ until $A_{600}$ of 0.3, centrifuged at 3,273 × *g* for 15 min at 4°C, and resuspended in CDM, with or without 100 μM $ZnSO_4$ and 0.1 μg.mL$^{-1}$ penicillin, either singly or in combination. Bacteria were incubated at 37°C + 5% $CO_2$ for 5 h, and the survival was assessed by determining the colony forming units (CFU) by 10-fold serial dilutions in 200 μL serum broth and plating 25 μl in technical duplicate spots on blood agar plates. Experiments were performed with three biological replicates. The relative survival was determined by the fold-change CFU for each sample compared with the untreated D39 wild-type strain using Microsoft Excel. The data was visualized and analyzed using GraphPad Prism 9.

### Development of resistance analyses

The development of resistance to antibiotics with and without PBT2 was undertaken as previously described (Ling et al., 2015). Succinctly, to investigate resistance development for *S. pneumoniae* strains D39 and 23F to PBT2 + ampicillin (Sigma-Aldrich), bacteria were sequentially passaged in CA-MHB. As a control for resistance development, the antibiotic vancomycin (Sigma-Aldrich) was used. Initially, the MIC for PBT2 with or without antibiotic was determined by broth micro dilution following CLSI guidelines in a microtiter plate. The highest antibiotic or PBT2 + antibiotic concentration that still showed growth after overnight incubation was diluted 1 in 250 into a new microtiter plate containing two-fold dilutions of antibiotic or PBT2 + antibiotic. This procedure was repeated until growth of the *S. pneumoniae* strains in PBT2 + ampicillin failed at 15–17 days. The assays were undertaken in biological triplicate.

### RNA sequencing and qRT-PCR

A stock solution of $ZnSO_4$ was prepared at a concentration of 100 mM in MilliQ water and sterilized using a 0.2 μm syringe filter. Gene expression was analyzed following growth of *S. pneumoniae* D39 to mid-logarithmic phase ($A_{600}$ = 0.3) in CDM with or without supplementation with 100 μM $ZnSO_4$. At mid-log phase ($A_{600}$ = 0.3), 500 μL of culture was mixed with 1 mL of RNA Protect (Qiagen) and cells were harvested via centrifugation before storage at −80°C. Bacterial pellets were RNA extracted and purified using RNeasy Protect Bacterial Mini kit (Qiagen) after enzymatic lysis using lysozyme and mutanolysin, all according to manufacturer's instructions. DNase treatment was performed on-column during RNA extraction using RNase-free DNase (Qiagen). Total RNA was determined for each sample using the NanoDrop spectrophotometer (ThermoFisher Scientific). Oligonucleotide primers for quantitative reverse transcription PCR (qRT-PCR) were designed in Primer3. The sequences were designed such that primers ranged from 18-20 bp in length, possessed a GC content of 40-60%, and amplified a 140–160 bp region specific to the gene of interest. Quantitative reverse transcription PCR was conducted in a 96-well plate with 10 ng total RNA per well using the Superscript III Platinum SYBR Green

One-Step qRT-PCR kit (Invitrogen) on a QuantStudio 7 Real-time PCR system (Applied Biosystems) as per manufacturer's instructions. The transcription levels of genes analyzed were normalized to those obtained for *gyrA* (primers listed in Table S6). The data was visualized and analyzed using GraphPad Prism 9. For RNA sequencing, RNA was extracted and prepared as above from biological quadruplicates of *S. pneumoniae strain* D39 or 23F. RNA was pooled and analyzed on a Bioanalyzer 2100 (Agilent) to confirm a RIN value >8 according to manufacturer's instructions. RNA was then submitted to Australian Genome Research Facility (AGRF) for sequencing. Briefly, the Epicentre Bacterial Ribozero Kit (Illumina) was used to deplete ribosomal RNA content before generation of barcoded libraries using Ultra Directional RNA kit (New England Biolabs). Prepared libraries were then sequenced using an Illumina HiSeq2500 with Version 3 SBS reagents and 2 × 100 bp single-end chemistry. Reads were aligned to the *S. pneumoniae* D39 (GenBank accession number NC_008533) or 23F (GenBank accession number FM211187) genome as appropriate using BOWTIE2 version 2.2.6 (Langmead and Salzberg, 2012). Counts for each gene were obtained using SAMtools version 1.2 (Li et al., 2009) and BEDtools version 2.24.0 (Quinlan and Hall, 2010), and differential gene expression was determined using R (DESeq Library) version 3.2.2 (Anders and Huber, 2010). Transcriptomic data has been deposited in the NCBI Gene Expression Omnibus databank under submission identifiers GSE159901 (D39) and GSE160372 (23F). RNA sequencing was validated by qRT-PCR analysis of *S. pneumoniae* strains grown under identical conditions to the RNA sequencing experiments in biological triplicate. Differential expression of genes analyzed were SPD_0382 (*fabK*), SPD_0526 (*fba*), SPD_0588 (*prtA*), SPD_0667 (*sodA*), SPD_0685 (*gor*), SPD_0789 (*pfkA*), SPD_0890 (*phtE*), SPD_1384 (*mntE*), SPD_1433 (*galT-2*), SPD_1463 (*psaA*), SPD_1634 (*galK*), SPD_1636 (*adhC*), SPD1637 (*nmlR*), and SPD_1638 (*czcD*) using primers listed in Table S6.

### Metabolomic sample preparation

*S. pneumoniae* D39 cultures for metabolomic analyses were grown as detailed above in biological quadruplicate in CDM ±100 μM $ZnSO_4$. At $A_{600}$ = 0.3, cultures were harvested by centrifugation at 7,000 × *g* for 7 min at 4°C. Once pelleted, cells were flash-frozen using liquid nitrogen to preserve the metabolite profile and stored at −80°C. Cultures were processed and analyzed via LC/MS by Metabolon, North Carolina, USA.

### GlmM and GlmU expression and purification

DNA sequences encoding GlmM (UniProtK – Q04J18) and GlmU (UniProt – Q04KU2) ordered from GenScript (Hong Kong) Ltd. in plasmid pUC57, were amplified *via* PCR and subcloned into pGEX-6P-1. The $GlmU_{E315AH330A}$ variant was generated using a Q5 Site-Directed Mutagenesis kit (New England BioLabs), according to the manufacturer's instructions using primers listed in Table S6. The plasmids were individually transformed into *E. coli* strain BL21 (DE3) (New England BioLabs). Cultures were grown at 37°C in Luria Broth (LB) supplemented with ampicillin (100 μg.mL$^{-1}$) to an $A_{600}$ of 0.6, induced with isopropyl β-D-1-thiogalactopyranoside (IPTG, 0.2 mM) and harvested after further incubation at 18°C for 20 h. Cell pellets expressing the GST-GlmM and GST-GlmU proteins were suspended in purification buffer (GlmM, 20 mM Tris pH 7.5, 150 mM NaCl; GlmU, 20 mM MOPS pH 7.0, 150 mM NaCl, 10% glycerol). The cell pellets were disrupted using a TS series bench top cell disruptor (Constant Systems Ltd) at 35 kpsi. Cell debris were removed by centrifugation (Beckman JLA-25.50, 30,000 × *g*, 20 min, 4°C). The soluble fractions of the cell lysates were incubated with glutathione sepharose 4B resin (GSH, Cytiva), pre-equilibrated with purification buffer. The GST tag was cleaved with PreScission Protease overnight at 4°C and the cleaved proteins were eluted by washing of the resin with purification buffer (20 column volumes). The cleaved proteins were concentrated by centrifugal ultrafiltration (Milipore Amicon Ultra 50 K MWCO) and further purified by SEC (HiLoad 16/600 Superdex 200 pg, Cytiva; purification buffer). The purified proteins were concentrated to 10 mg.mL$^{-1}$ before storage at −80°C.

### GlmM and GlmU enzyme activity assays

The glucosamine-6-phosphate (GlcN-6-P) mutase activity of GlmM was assayed essentially as described (Li et al., 2012) using a coupled assay system in which glucosamine-1-phosphate (GlcN-1-P) is converted from GlcN-6-P by the mutase and then quantitatively converted into UDP-N-acetyl-glucosamine (UDP-GlcNAc) in the presence of purified GlmU. The by-product of GlmU catalyzed acetyltransferase activity was measured by a colorimetric assay coupled with 5, 5′-dithio-bis-(2-nitrobenzoic acid) (DTNB). The 50 μL reaction mixture contained 50 mM Tris HCl, pH 7.5, 5 mM $MgCl_2$, 2 mM acetyl CoA (Merck), 0.4 mM GlcN-6P (Merck), purified GlmM (1 μg), and purified GlmU (2 μg), in a 96-well microtiter plate. The reaction was incubated at 37°C for 10 min and terminated by adding 50 μL of a stop solution (50 mM Tris-HCl, pH 7.5, 6 M guanidine hydrochloride) and then incubated for 10 min with 50 μL Ellman's reagent solution (0.2 mM DTNB, 50 mM Tris-HCl, pH 7.5, 1 mM EDTA). Absorbance readings at 412 nm were collected using a FLUOstar Omega microplate reader (BMG Labtech) and the molar absorption coefficient for $TNB^{2-}$ (13,700 $M^{-1}$ $cm^{-1}$) used to calculate the concentration of CoA, which is proportional to the number of acetylated glucosamine-1-phosphate molecules produced during the reaction. Zinc inhibition of GlmM activity was assessed by pre-incubation of the protein at fixed concentrations of $ZnCl_2$ (5 μM, 10 μM and 20 μM) for 15 min prior to the enzymatic assays. The GlcN-1-P acetyltransferase activities of the GlmU and the $GlmU_{E315AH330A}$ variant were measured using a similar assay system comprising 50 mM Tris–HCl pH 7.5, 5 mM $MgCl_2$, 0.4 mM GlcN-1-P (Merck), 1 mM acetyl CoA (Merck), and 40 ng purified GlmU (wild-type GlmU or $GlmU_{E315AH330A}$). Reactions were incubated in a 96-well microtiter plate (37°C, 10 min), terminated and absorbance at 412 nm read. The N-acetylglucosamine-1-phosphate uridyltransferase activity of GlmU was determined using a malachite green colorimetric assay (Zhou et al., 2011). The reaction mixture (80 μL) contained 50 mM Tris–HCl, pH 7.5, 10 mM $MgCl_2$, 10% (v/v) glycerol, 1 mM dithiothreitol, 0.4 mM GlcNAc-1-P, 0.4 mM UTP,

0.04 units of pyrophosphatase, and 0.1 μg purified GlmU protein and was incubated in 96-well microtiter plate at 37°C for 10 min. The reaction was then stopped by addition of 80 μL of color reagent [0.03% (w/v) malachite green, 0.2% (w/v) ammonium molybdate, 0.05% (v/v) Triton X-100 in 0.7 M HCl]. The reaction was incubated for 5 min at 37°C and absorbance monitored at 630 nm using a FLUOstar Omega microplate reader. Assays were supplemented with $ZnCl_2$ (final concentrations 5–20 μM) in order to determine whether the enzyme activities were affected by interaction with Zn ions. Experiments were performed in triplicate and data fit by nonlinear regression using the Michaelis-Menten or uncompetitive inhibition kinetic models to derive $K_m$ and $V_{max}$ parameters in GraphPad Prism (version 9).

### Metal content analysis of GlmU proteins

The metal content of the purified metal-loaded GlmU proteins was determined by ICP-MS. The GlmU protein (2.5 μM) in buffer (20 mM Tris-HCl, pH 7.0, 200 mM NaCl, 10% glycerol, 5 mM TCEP) was digested in 200 μL of 35% $HNO_3$ (Merck Suprapur, Australia), diluted to a final volume of 1 mL using MilliQ $H_2O$ and heated at 96°C for 15 min. Insoluble material was removed by centrifugation at 18,000 × *g* for 25 min. Technical triplicate measurements of samples and controls were analyzed on an Agilent 8900 Triple Quadrupole ICP-MS with a MicroMist nebulizer (Glass Expansion, Australia). Torch positioning, sample depth adjustment and lens optimization were set according to manufacturer recommendations, while other instrumental parameters were optimized during a batch-specific user tune. Helium collision gas flow rate of 5 $mL.min^{-1}$ was used to minimize polyatomic interferences. Samples were introduced via an integrated automation system (IAS) autosampler (Agilent) using a peristaltic pump.

### GlmU crystallization, data collection, structure solution and refinement

The GlmU-acetyl CoA-$Zn^{2+}$ complex was crystallized by hanging drop vapor diffusion in 24-well VDX plates (Hampton Research) using a condition adapted from that reported (PDB 1HM8 (Sulzenbacher et al., 2001)). Equal volumes of protein sample (2 μL; 15 $mg.mL^{-1}$, 20 mM MOPS pH 7.5, 0.15 M NaCl, pre incubated with 20 mM acetyl CoA) and reservoir solution (20 mM Tris-HCl, pH 7.2, 20% (v/v) PEG 400, 50 mM NaCl, 300 mM $CaCl_2$, and 1 mM $ZnCl_2$), were equilibrated against reservoir solution (0.5 mL). Rhombohedral crystals appeared within one week. Crystals were flash-cooled in liquid nitrogen and diffraction data from a single crystal were recorded on an Eiger 16 M detector at the Australian Synchrotron, beamline MX2. In order to unequivocally identify the $Zn^{2+}$ binding site in the GlmU structure, diffraction data were collected at three energies at or remote from the Zn K-edge (Table 1, Native, High energy, Low energy). The data were indexed and integrated with XDS (Kabsch, 2010) and scaled with AIMLESS (CCP4, 1994; Evans and Murshudov, 2013). Anomalous difference Fourier maps were calculated with FFT (Figures S1C and S1D). The crystal structure of GlmU-acetyl CoA-$Zn^{2+}$ was solved by molecular replacement using the program PHASER (McCoy et al., 2007). The crystal structure of GlmU-acetyl CoA [PDB 1HM8, (Sulzenbacher et al., 2001)] was used as the search model after removal of all water molecules. Manual model building and the addition of water molecules were carried out in COOT (Emsley and Cowtan, 2004). The model was refined using REFMAC5 (Murshudov et al., 2011) and the quality of the structure was determined by MOLPROBITY (Chen et al., 2010).

### GlmU residue conservation analysis

Publicly available database of 20,010 *S. pneumoniae* genomes was obtained from (Gladstone et al., 2019) and were assembled using shovill v.1.0.9 (Hayes et al., 2020) with an underlying SKESA v.2.3.0 assembler (Souvorov et al., 2018). The *Streptococcus pneumoniae* D39 genome (NC_008533.gbk) served as the reference genome to determine the presence, amino acid sequence and alignment of spd_0874 (*glmU*) across the 20,010 clinical isolates using the screen_assembly script (Davies et al., 2019) and BLASTN v2.9.0 with parameters of 80% coverage and 80% identity. Amino acid variation was determined using MUSCLE alignment in Geneious Prime (Kearse et al., 2012). Sequence conservation, as determined by percentage of variant amino acids compared to consensus, was rendered onto the GlmU crystal structure (PDB 1G95) using UCSF Chimera (Pettersen et al., 2004).

### Scanning electron microscopy (SEM)

SEM studies were undertaken at the Centre for Microscopy and Microanalysis at the University of Queensland. Bacterial strains were cultured in CA-MHB ($A_{600}$ = 0.4) and treated in the absence and presence of PBT2 (0.4 μM) and $ZnSO_4$ (50 μM) for 24 h at 37°C. Bacteria were washed twice with PBS preceding glutaraldehyde fixation. Samples were then dehydrated, assisted with a Pelco biowave regimen, via a series of ethanol treatments (30-100% (v/v) ethanol), one treatment with 100% ethanol/hexamethyldisilazane (HMDS; 1:1) and finally, two treatments with 100% HMDS. Samples were applied to coverslips coated with 1 $mg.mL^{-1}$ poly-*L*-lysine before being air dried for 2 h. Coverslips were attached to 13 mm SEM-stubs with double-sided carbon tabs, plasma-cleaned for 10 min in an Evactron E50 De-contaminator (XEI Scientific) and coated with two layers of platinum (first layer 0° angle from above, second layer 45° angle from above) using a Q150T Turbomolecular pumped coater (Quorum Tech) following manufacturer's instructions. Samples were imaged in a JEOl JSM 7100F or JEOl JSM 7800F field emission SEM (JEOL) at an accelerating voltage of 1-3 kV.

### Peptidoglycan detection assay

Detection of peptidoglycan was conducted using a muramic acid quantitation protocol modified from (Hadžija, 1974). *S. pneumoniae* was grown to mid-log phase ($A_{600}$ = 0.3) in 10 mL CDM with or without supplementation of 50 μM $ZnSO_4$, 0.4 μM PBT2.2HCl, either singly or in combination. Biomass from 1 mL of each culture was harvested by centrifugation at 18,000 × *g* for 4 min and washed once

in 1 mL sterile PBS with 20 μL taken for CFU enumeration. The cell pellets were resuspended in 100 μL 1 M NaOH and left to incubate at 38°C for 30 min, prior to addition of 100 μL 0.5 M $H_2SO_4$ and 1 mL concentrated $H_2SO_4$ (~18 M). Samples were incubated at 96°C for 7 min and cooled on ice prior to addition of 10 μL 4% (w/v) $CuSO_4$ and 20 μL 1.5% (w/v) 4-phenylphenol in 96% ethanol with immediate mixing. Samples were then incubated for a further 30 min at 30°C before determination of $A_{560}$ in a clear, 96 well plate using a CLARIOstar spectrophotometer (BMG Labtech). CFU were enumerated after overnight growth on BA plates at 37°C + 5% $CO_2$ and $A_{560}$ was corrected for CFU.mL$^{-1}$ for each culture and normalized to untreated.

### Fluorescence polarization assay

The Zn reporter strain was constructed by amplifying the promoter region of *czcD* from D39 genomic DNA using oligonucleotides P*czcD*-F and *czcD*-R, *hlpA*-GFP from a GFP PCR construct (Kjos et al., 2015) using oligonucleotides GFP-P*czcD*-F and GFP-R, a spectinomycin resistance cassette from pABG5-3 mini using Spec-F and Spec-R, and flanking regions from spd_1789 using SPD1789-US-F, 1789-US-P*czcD*-R, SPD1789-DS-F and SPD1789-DS-R (primer sequences are listed in Table S6). The fragments were ligated using NEBuilder HiFi DNA Assembly Master Mix (New England Biolabs) and transformed into *S. pneumoniae* D39 containing a P*hlpA-hlpA_hlpA-rfp*_Cam$^r$ construct (Kjos and Veening, 2014), which constitutively expresses far-red fluorescent protein mKate2. The Mn reporter strain was similarly constructed using oligonucleotides P*psaBCA*-F and P*psaBCA*-R to amplify the *psaBCA* promoter region and fuse with P*psaBCA*-F and P*psaBCA*-R, *hlpA*-GFP, from a GFP PCR construct (Kjos et al., 2015) using oligonucleotides GFP-P*psaBCA*-F and GFP-R, and a spectinomycin resistance cassette from pABG5-3 mini, using Spec-F and Spec-R and flanking regions from spd_1789 using SPD1789-US-F, SPD1789-US-P*psaBCA*-R, SPD1789-DS-F, and SPD1789-DS-R (Table S6). *S. pneumoniae* strains were grown to mid-log ($A_{600}$ = 0.3) in Todd-Hewitt Broth (THY) and used to inoculate C+Y medium containing 0.4 μM PBT2 and/or 50 μM $ZnSO_4$ to an $A_{600}$ = 0.01. Cultures were added to a black walled, clear bottom 96-well plate with a BreathEasy gas permeable seal (Diversified Biotech). A CLARIOstar microplate reader (BMG Labtech) at 37°C, 5% $CO_2$ was then used to measure optical density ($A_{600}$) and fluorescence polarization (Ex 482-16/Em 530-40 with dichroic filter LP 504). Optical density measurements were used to identify the mid-point of the exponential growth phase for each culture to determine the fluorescence polarization (*mP*) values. Assays were performed in biological triplicate.

### Murine challenge experiments

For these experiments 8-week old female BALB/c were utilized. *S. pneumoniae* strain DAW30 was grown in 5% $CO_2$ at 37°C on tryptic soy agar (TSA) plates supplemented with 3% sheep blood and 20 μg.mL$^{-1}$ neomycin, in a semi-defined media C+Y. Bacteria were grown to mid-logarithmic phase ($OD_{620}$ ~ 0.4) in 10 mL C+Y and diluted in PBS according to a previously determined standard curve. Bacteria were enumerated on TSA blood agar plates to confirm the correct number was used for infection. Mice were infected with 5 × $10^5$ colony forming units (CFU) in 100 μL intranasally (IN) of *S. pneumoniae* strain DAW30. The treatment groups were SSV (0.9% NaCl (w/v), 0.5% (w/v) sodium-carboxymethylcellulose, 0.5% (v/v) benzyl alcohol, 0.4% (w/v) Tween-80) 100 μL by oral gavage (treated at infection and 6 h post-infection [PI]), PBT2 100 μL oral gavage (treated at infection, 6 h PI), PBT2 100 μL oral gavage and 100 μL subcutaneous ampicillin (treated at infection and 6 h PI), and ampicillin 100 μL subcutaneous (treated at infection and 6 h PI). PBT-2 was reconstituted at 30 mg in 10 mL (15 mg.kg$^{-1}$ in 100 μL x 2 treatments/day) in SSV and sonicated for 5 minutes to solubilize compound. Ampicillin was made at 50 mg in 10 mL (25 mg.kg$^{-1}$ per 100 μL) in $ddH_2O$. At 24 h lungs were harvested and plated on blood agar plates for bacterial load assessment. Experimental groups consisted of five mice per treatment group that was repeated twice for a total of ten mice in each experimental treatment group.

### Ethics statement

All experiments involving animals were performed with prior approval of and in accordance with guidelines of the St. Jude Institutional Animal Care and Use Committee. The St Jude laboratory animal facilities have been fully accredited by the American Association for Accreditation of Laboratory Animal Care. Laboratory animals were maintained in accordance with the applicable portions of the Animal Welfare Act and the guidelines prescribed in the DHHS publication, Guide for the Care and Use of Laboratory Animals. All mice were maintained in BSL2 facilities, and all experiments were done while the mice were under inhaled isoflurane (2.5%) anesthesia. Mice were monitored daily for signs of infection and disease progression. This work was approved under the IACUC protocol number 538-100013-04/12 R1.

## QUANTIFICATION AND STATISTICAL ANALYSIS

Statistical details for each experiment can be found in the corresponding figure legends with error bars representing either S.E.M. or S.D. as noted. A minimum of three experimental replicates were performed for each assay, and the number of replicates is noted in the corresponding figure legend. All p values were calculated using a one-way analysis of variance (ANOVA) (with Tukey multiple comparisons test), two-tailed unpaired *t*-test, or log-rank (Mantel-Cox) test when applicable. Statistical work was performed using Prism 9 software (GraphPad), and significance is indicated on the graphs as follows: not significant (ns) = $p > 0.05$; * = $p < 0.05$; ** = $p < 0.01$; *** = $p < 0.001$; **** = $p < 0.0001$.